Energy 180 (2019) 272–291

Contents lists available at ScienceDirect

Energy

journal homepage: www.elsevier.com/locate/energy

On the response of a lean-premixed hydrogen combustor to acoustic and dissipative-dispersive entropy waves

A. Fattahi [a, *], S.M. Hosseinalipour [b], N. Karimi [c], Z. Saboohi [d], F. Ommi [d, e]

[a] Department of Mechanical Engineering, University of Kashan, Kashan, Iran
[b] School of Mechanical Engineering, Iran University of Science and Technology, Tehran, Iran
[c] School of Engineering, University of Glasgow, Glasgow, G12 8QQ, United Kingdom
[d] Aerospace Research Institute (ARI), Ministry of Science, Research and Technology, Tehran, Iran
[e] Department of Mechanical Engineering, Tarbiat Modares University, Tehran, Iran

ARTICLE INFO

Article history:
Received 13 October 2018
Received in revised form
13 March 2019
Accepted 27 April 2019
Available online 8 May 2019

Keywords:
Hydrogen combustor
Thermoacoustic instability
Convective instability
Entropy waves
Wave dissipation and dispersion
Indirect combustion noise

ABSTRACT

Combustion of hydrogen or hydrogen containing blends in gas turbines and industrial combustors can activate thermoacoustic combustion instabilities. Convective instabilities are an important and yet less investigated class of combustion instability that are caused by the so called “entropy waves”. As a major shortcoming, the partial decay of these convective-diffusive waves in the post-flame region of combustors is still largely unexplored. This paper, therefore, presents an investigation of the annihilating effects, due to hydrodynamics, heat transfer and flow stretch upon the nozzle response. The classical compact analysis is first extended to include the decay of entropy waves and heat transfer from the nozzle. Amplitudes and phase shifts of the responding acoustical waves are then calculated for subcritical and supercritical nozzles subject to acoustic and entropic forcing. A relation for the stretch of entropy wave in the nozzle is subsequently developed. It is shown that heat transfer and hydrodynamic decay can impart considerable effects on the entropic response of the nozzle. It is further shown that the flow stretching effects are strongly frequency dependent. The results indicate that dissipation and dispersion of entropy waves can significantly influence their conversion to sound and therefore should be included in the entropy wave models.

1. Introduction

Noise emitted by the power generating devices is deemed an important environmental pollution, and there is an increasing emphasis on making these systems quieter [1]. In gas turbines, the noise generated by the combustion of fuel has been identified as a major contributor to the total noise emitted from the unit [2,3]. Further, combustion generated noise can sometimes contribute with the so called thermoacoustic instabilities [3,4]. These instabilities include strong pressure oscillations, which can induce pronounced mechanical vibrations and lead to hardware damage [4]. Avoiding thermoacoustic instabilities is, currently, a major challenge before the development of clean gas turbine combustors [4]. It follows that understanding and modelling of combustion generated noise is a crucial element for the future advancements of gas turbine combustion technologies [5,6].

Combustion noise is, broadly, divided into direct and indirect components [1,2]. Direct combustion noise arises from the fluctuations in the flame heat release, mainly caused by the turbulence in the flow or interaction of the flame with acoustics [1,2]. This topic has been studied extensively through numerical simulations [3,7,8] and experiments [2,9–11]. Indirect combustion noise, however, is relatively less explored. The generation of sound by this mechanism is due to the conversion of density inhomogeneities into acoustic waves, which often occurs in a downstream nozzle. As a result, this mechanism, also called entropy noise, includes post flame interactions mainly within the exit nozzle of the combustor [1]. The physical principles of entropy noise were explained by Ffwocs Williams and Howe [12] and Howe [13] in the seventies. They showed that convection of low density fluid parcels through a region of mean pressure gradient, can generate sound [12,13]. Such parcels of low density fluid or hot spots, often called entropy waves, can be readily generated in a gas turbine combustor [4]. The process of conversion of entropy waves to acoustic waves was first

* Corresponding author.
E-mail addresses: afattahi.mech@gmail.com, afattahi@kashanu.ac.ir (A. Fattahi).

https://doi.org/10.1016/j.energy.2019.04.202

modelled by Marble and Candel [14]. In their seminal work, these authors derived analytical expressions for the reflected and transmitted acoustic waves, generated by the passage of entropic and acoustic waves through a nozzle [14]. Their analysis was one-dimensional, fully linear and on the basis of compactness of the nozzle and Euler equations [14]. Although they did not present any comparison, the subsequent studies confirmed the validity of their results. Cumpsty and Marble [15] extended the analysis of Marble and Candel [14] to a turbine stage as a quasi-two-dimensional domain. The comparison between the analytical results and experimental data obtained from a Rolls-Royce aero-engine revealed maximum 50% error for the predicted entropy wave. They found that the entropy noise is strongly affected by the pressure ratio in each stage [15]. Later, Cumpsty [16] theoretically compared pressure, entropy and vorticity noise in an unsteady combustion and estimated that entropy noise dominates the total noise emission. The analysis was in qualitative agreement with the experiments on an aero-engine.

Recently, these models were extended to less restrictive conditions and examined more thoroughly in a series of work by various authors. Stow et al. [17] conducted a frequency asymptotic expansion of the flow perturbations and introduced the concept of effective length of the nozzle. They, therefore, released the assumption of nozzle compactness in the analysis of Marble and Candel [14] and calculated the reflection characteristics of an annular nozzle [17]. These authors used a numerical solver to compare the analytical results and very good agreement was found for the frequencies below 1 Hz. A similar approach was taken by Goh and Morgans [18] in their quasi one-dimensional analysis of a non-compact nozzle. These authors derived theoretical expressions for the phase of the transmission coefficients due to an incident acoustic or entropic wave and compared those with numerical simulations [18]. Moase et al. [19] used hypergeometric functions in their quasi-one-dimensional, analytical investigation of the dynamic response of a nozzle. In their analysis, the nozzle could have an arbitrary shape and be subject to acoustic and entropic excitation [19]. A quasi one-dimensional Euler solver with an adapted nonlinear artificial dissipation model was used to validate the analytical solution. Moase et al. [19], further, investigated the effects of nonlinearities and developed a method to quantify the level of nonlinearity [19]. Hosseinalipour et al. numerically showed that the assumption of passive scalar in analysis of entropy waves is largely incorrect [20].

The comprehensive measurements of Bake and his co-workers [21,22] provided experimental data on entropy noise and increased the theoretical interest in this problem. Leyko et al. [23] conducted Large Eddy Simulation (LES) of Bake et al. experiment [22] along with analytical compact analysis. They concluded that the compact analysis of Marble and Candel was capable of predicting the experimental results of Bake et al. [22]. In a combined analytical and numerical investigation, Duran et al. [24,25] considered the subsonic case in Bake et al. experiment [22]. They showed that the compact model of Marble and Candel [14] can only predict the noise generation at low Mach numbers in their case studies [24,25]. Duran and Moreau [26] used Magnus expansion to release the assumption of compactness in the acoustic and entropic analyses of nozzles. The analytical relations were validated against the results of Marble and Candel [14] for the case of a nozzle with a linear steady velocity profile. They derived analytical expressions for the dynamic response of the transmitted noise and showed that this is highly frequency dependent [26]. The compact analysis of Ref. [14] has been further extended to include high amplitude acoustic and entropic waves through a second order, nonlinear analysis [27].

Over the last few decades, the theoretical results of Marble and Candel [14] have extensively been employed in the numerical and theoretical studies of combustion noise and thermoacoustic instabilities [25]. Despite this, the practical significance of entropy waves in both of these topics is still being debated. For instance, in a theoretical study, Leyko et al. [28] showed that the ratio of indirect to direct combustion noise depends upon the Mach numbers in the flame region and nozzle. They then argued that comparing to direct combustion noise, indirect noise is insignificant in small scale combustors, but becomes appreciable in gas turbines [28]. Further, Duran and Moreau [26] demonstrated that the ratio of indirect to direct noise decreases at higher frequencies. They, therefore, confirmed the argument made by other authors on the limitation of the effects of entropy waves to low frequencies [26]. Similar conclusion was made by Fattahi et al. [29] in their recent numerical simulation of entropy wave propagation. These authors further showed that advection of entropy waves in heat transferring flows is associated with significant dissipation and dispersion [29].

The influence of entropy noise on thermoacoustic instabilities has been, particularly, a matter of contention. Dowling and her co-worker experimentally [30] and theoretically [31] demonstrated that the downstream boundary condition of a combustor could be thermo-acoustically destabilising. Keller [32] proposed a model for the frequency of entropically driven instabilities in a gas turbine premixed combustor with chocked exit. According to Keller's model [32], the main driver of instabilities is the acoustic waves generated by the convection of entropy disturbances through the downstream chocked nozzle. Similar arguments were made by Zhu et al. [33] in their numerical simulation of a spray combustor. Polifke et al. [34] developed a linear model for the thermoacoustics of a premixed combustor with chocked exit. These authors showed that the interactions between the generated entropy waves and the chocked exit nozzle could alter the thermoacoustic stability of the system [34]. This was later confirmed by the experiments of Hield et al. [35] on a thermoacoustically unstable, premixed combustor with open and choked exit nozzles. Hield et al. [35], further, showed that through the inclusion of dispersive entropy waves and the boundary conductions of Marble and Candel [14], the observed thermoacoustic instability could be successfully modelled. They, therefore, concluded that entropy waves are of significance in thermoacoustic stability of combustors [34]. However, Eckstein et al. [36,37] made a totally different conclusion from their experimental and modelling works on a liquid fuel combustor. They considered the dispersion of entropy waves and argued that entropy waves make a negligible contribution with the thermoacoustic instability of the combustor [36]. Their model for the dispersion of entropy wave was developed in the earlier work of Sattelmayer [38], who modelled the dispersing process as a temporal stretch of a density impulse. This analysis was on the basis of the residence time distribution in a simple exhaust duct [38]. The probability density function (p.d.f) of this residence time was used to model the dispersion process [38]. Sattelmayer [38] argued that non-uniformity of a duct flow can cause significant dispersion and hence, entropy waves could hardly survive in real combustors. He, therefore, considered entropy waves to be of little significance in the analysis of thermoacoustic instabilities [38]. The opposing statements made in Refs. [35,36,37] could be due to the effects of flow on entropy waves. As Fattahi et al. [29] demonstrated, the thermal and hydrodynamic conditions of the flow can significantly affect the entropy wave. Since the extent of these effects heavily depends on the convecting time scale [29], they are expected to be more pronounced in the long combustion tube of Eckstein et al. [36,37] in comparison to the short-length rig of Hield. et al. [35].

Similar to the numerical results reported in Refs. [36,37], experimental studies of entropy waves inside thermoacoustically unstable combustors have confirmed that entropy waves could be

highly dispersive [39,40]. However, the recent direct numerical simulation of Morgans et al. [41] in an incompressible, non-reactive, channel flow showed that entropy waves could mostly survive the flow decay and dispersion effects. These authors rebutted the conclusion made by Sattelmayer [38] due to defects in applying p.d.f [41] and argued that the correct p.d.f should be Gaussian-like rather than a rectangular distribution as used by Sattelmayer [38]. The conclusion made by Morgans et al. [41] shows that non-physical assumptions made in the analyses of entropy waves could be partially responsible for inconsistency in the literature. Similarly, Domenic et al. [42–45] in a series of analytical and experimental works, showed that the analytical model for prediction of acoustics of a subsonic flow can be defective without a reverberation. Another potential source of contention could be the pressure loss in the nozzle, which has been recently incorporated by Domenic et al. [42–45] into the entropy wave conversion models. These authors measured the reflection coefficient and clearly separated indirect and direct noise [43]. It was shown that the indirect noise in both up-warding and down-warding directions should not be neglected, particularly at sonic nozzle conditions [43,44]. Domenic et al. [43] also concluded that probable merging in measurement of direct and indirect noise might be the reason of dismissing entropy noise in some studies.

Following the work of Morgans et al. [41], Wassmer et al. [46] developed a linear one-dimensional convective-diffusive model of entropy waves, in which effective diffusivity was inferred from experimental data [46]. The theoretical investigation of Goh and Morgans [47] showed that introducing decay and dispersion of entropy waves could significantly modify the thermoacoustic instability of the system. These authors considered a simple thermoacoustic model of a premixed combustor [47] and added decaying and dispersive entropy waves to the system [47]. They showed that depending upon the strength of the decay and dispersion of entropy waves, thermoacoustic instability could be either encouraged or discouraged [47]. In a recent large eddy simulation of an aero-engine combustor, it was shown that entropy waves shift the eigen modes of the system to higher frequencies and could cause mixed acoustic-entropic instabilities [48]. Further, Lourier et al. [49] emphasised the effect of the shape of entropy waves on the peak pressure fluctuations. They argued that the shallower shaped entropy wave generate smaller peaks in the pressure wave [49]. This finding was a strong evidence for the influence of dispersion mechanisms on the entropy noise. Recently, Magri et al. [50] introduced a new source of entropy fluctuations in combustors, referred to as compositional wave, caused by the chemical potential of an incomplete mixing. This source of entropy wave could be another reason for the difference between the analytical results and experimental data reported in literature. Following the work of Marble and Candel [14], Magri et al. extended compact relations for both supercritical and subcritical nozzles [50]. The validity of their approach was confirmed in the limits of uniform Mach number at the nozzle inlet and outlet and no compositional fluctuations. They concluded that chemical potential of gases can change through the nozzle resulting in an additional source of entropy disturbances [50].

The preceding review of literature clearly showed that the decay and dispersion of entropy waves could significantly affect indirect combustion noise and thermoacoustic stability of the combustor. However, the extents of these effects are, currently, unknown. This has resulted in significant disagreements in the literature and caused confusion about the practical significance of entropy waves. An essential step in improving the situation is to detect all the possible mechanisms of decay and dispersion of entropy waves and include them in the thermoacoustic models of combustors. In general, there exist two mechanisms of decay and dispersion of entropy waves. These are due to hydrodynamics and heat transfer [29]. The former can decay the entropy wave by viscous dissipation and turbulent mixing and also disperse the wave by the spatial non-uniformities of the velocity field. Transfer of heat from the combustor and nozzle can also modify acoustic and entropic waves. Further, it can affect the velocity field in compressible flows and therefore leave an indirect influence on the acoustic and entropic waves [48,49]. In reality, all combustors and exit nozzles include heat transfer and hydrodynamic effects. This raises the question that whether these effects should be involved in the low order thermoacoustic models of combustors.

The problems of heat transfer and hydrodynamic dispersions in ducts have received some attention in the literature [29,38,49–52]. In particular, Karimi et al. [51,52] and Fattahi et al. [29] have demonstrated the significant effects of heat transfer upon the reflection and transmission of the resultant sound waves, and the survival of entropy waves. Howe [53] elaborated on the stretch effects by calculating the stretch of the entropy waves in Bake's experiment [22]. Further, Goh and Morgans [19] denoted the importance of stretch of entropy waves upon the dynamic response of the nozzle. However, they did not consider this effect in their analysis. The significance of the dissipation and dispersion of entropy waves have been noted by a number of authors in their analytical [18,54], numerical [41,47] and experimental [37] investigations and also in the reviews of the subject, see for example [1,54]. Despite these, so far most of the analyses of nozzle response, including the early ones [14,15] and their more recent extensions [17–19,26,27], have totally ignored the decay and dispersion of entropy waves. So far, a systematic evaluation of these effects upon the acoustic and entropic responses of nozzles has not been reported. To address this issue, the current study adds the dissipation and dispersion of the entropy waves to a predictive model of indirect combustion noise. This is achieved by considering the hydrodynamic and thermal effects of the flow field on entropy waves and further allowing for the entropy wave stretch in the nozzle. Prediction of the phase shift by considering the concept of 'effective length' in a non-compact nozzle with a finite length is another advantage of the current analytical approach.

2. Problem configuration and the governing equations

In the current work, a convergent-divergent nozzle shown in Fig. 1 is considered. The convergent and divergent parts are respectively called throat upstream and downstream. An incident entropic (σ) or acoustic incident wave (P_1^+) enter the nozzle and this generally produces three acoustic waves: P_1^-, P_2^+ and P_2^-. In here, indices 1 and 2 stand for the upstream and downstream of the throat, respectively. In addition, + and − symbols indicate the waves travelling towards the downstream and upstream directions.

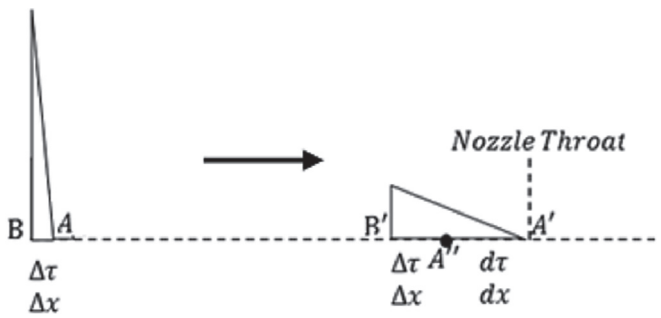

Fig. 1. The schematic configuration of the nozzle illustrating the propagating and convecting waves.

In keeping with the literature [23–26], the section of the nozzle located upstream of the throat is much shorter than the downstream part.

The proceeding analyses include the following assumptions.

(a) The steady heat transfer is assumed to be purely radiative,
(b) cooling does not change the critical statue of the nozzle,
(c) there is no shock wave in the divergent part of the supercritical nozzle,
(d) there are no frictional losses and the unsteady heat transfer is negligible,
(e) The working fluid is the product of a lean-premixed hydrogen combustion given by Eq. (73),
(f) the working fluid is an inviscid, non-heat-conducting, ideal gas,
(g) the supercritical cases exclude shock waves,
(h) the combustion products are completely mixed.

The one-dimensional conservation equations of mass, momentum and energy are [48].

$$\frac{1}{\rho}\left(\frac{\partial \rho}{\partial t}+u\frac{\partial \rho}{\partial x}\right)+\frac{\partial u}{\partial x}=0, \tag{1}$$

$$\frac{\partial u}{\partial t}+u\frac{\partial u}{\partial x}+\frac{1}{\rho}\frac{\partial p}{\partial x}=0, \tag{2}$$

$$\frac{Ds}{Dt}=\frac{q}{\rho T}. \tag{3}$$

In the above equations, p, ρ, u, s and t are respectively the static pressure (Pa), fluid density (kg/m^3), velocity (m/s), entropy (kJ/kgK) and time (s). Further, T is the fluid absolute temperature (K) and q is the heat addition or loss per unit volume (W/m^3).

Flow variables are then substituted by the summation of the steady and perturbation parts such that $g=\overline{g}+g'$, in which g is a flow property. Ignoring the second order terms results in the linearized form of mass, momentum and energy equation (1)- (3). These are [18].

$$\left(\frac{\partial}{\partial t}+\overline{u}\frac{\partial}{\partial x}\right)\frac{\rho'}{\overline{\rho}}+\overline{u}\frac{\partial}{\partial x}\left(\frac{u'}{\overline{u}}\right)=0, \tag{4}$$

$$\frac{\partial}{\partial t}\left(\frac{u'}{\overline{u}}\right)+\overline{u}\frac{\partial}{\partial x}\left(\frac{u'}{\overline{u}}\right)+\frac{\rho'}{\overline{\rho}}\frac{\partial \overline{u}}{\partial x}+2\overline{\rho u}\frac{u'}{\overline{u}}\frac{\partial \overline{u}}{\partial x}+\overline{p}\frac{\partial}{\partial x}\left(\frac{p'}{\overline{p}}\right)+\frac{p'}{\overline{p}}\frac{\partial p'}{\partial \overline{p}}=0, \tag{5}$$

$$\frac{Ds'}{Dt}=\frac{\overline{q}R}{\overline{p}}\left(\frac{q'}{\overline{q}}-\frac{u'}{\overline{u}}-\frac{p'}{\overline{p}}\right). \tag{6}$$

It, further, follows from the first law of thermodynamics that [41].

$$\frac{s'}{c_p}=\frac{p'}{\gamma p}+\frac{\rho'}{\rho}. \tag{7}$$

Combining Eqs. (4), (6) and (7) yields

$$\left(\frac{\partial}{\partial t}+\overline{u}\frac{\partial}{\partial x}\right)\left(\frac{p'}{\gamma \overline{p}}\right)+\overline{u}\frac{\partial}{\partial x}\left(\frac{u'}{\overline{u}}\right)=\frac{\overline{q}R}{\overline{p}}\left(\frac{q'}{\overline{q}}-\frac{u'}{\overline{u}}-\frac{p'}{\overline{p}}\right). \tag{8}$$

The acoustic waves are assumed to be planar and propagating in both directions of the one-dimensional domain. Thus [18],

$$\frac{p'}{\gamma \overline{p}}=P^{+}\exp\left(i\omega\left[t-\frac{x}{\overline{u}+c}\right]\right)+P^{-}\exp\left(i\omega\left[t-\frac{x}{\overline{u}-c}\right]\right), \tag{9}$$

$$\frac{u'}{c}=U^{+}\exp\left(i\omega\left[t-\frac{x}{\overline{u}+c}\right]\right)+U^{-}\exp\left(i\omega\left[t-\frac{x}{\overline{u}-c}\right]\right), \tag{10}$$

in which ω is the angular frequency and the superscripts $+$ and $-$ respectively denote downstream-travelling and upstream-travelling waves. Further, the convected entropy wave can be presented as

$$\frac{s'}{c_p}=\sigma\exp\left[i\omega\left(t-\frac{x}{u}\right)\right]. \tag{11}$$

By substitution of the harmonic solutions for the pressure and velocity into Eqs. (4) and (8), the following expressions can be developed.

$$\rho^{+}=U^{+}, \tag{12-a}$$

$$\rho^{-}=-U^{-}, \tag{12-b}$$

$$U^{+}=P^{+}, \tag{12-c}$$

$$U^{-}=-P^{-}, \tag{12-d}$$

$$q^{+}=P^{+}\left(\gamma+\frac{1}{M}\right)+P^{-}\left(\gamma-\frac{1}{M}\right). \tag{12-e}$$

Due to the fixed geometry of the nozzle, the mass variation at the inlet and outlet are identical. Hence,

$$\frac{1}{M}\left(\frac{u'}{c}\right)+\frac{\rho'}{\overline{\rho}}=const. \tag{13}$$

Because of the heat transfer effects on the entropy waves, an energy balance should be introduced. This is [50].

$$\dot{q}=\dot{m}C_p(T_{t2}-T_{t1}) \tag{14}$$

where T_t, $\dot{m}$ and $\dot{q}$ are the stagnation temperature (K), mass flow rate (kg/s) and heat transfer rate (W). Linearizing Eq. (14) and considering $\left(\frac{\acute{m}}{\overline{m}}\right)_1=\left(\frac{\acute{m}}{\overline{m}}\right)_2$ [23] for the two parts of the nozzle reveals that

$$\frac{T'_{t1}}{\overline{T}_{t1}}+\frac{\acute{q}}{\overline{m}C_p\overline{T}_{t1}}=\frac{T'_{t2}}{\overline{T}_{t2}}\left(1+\frac{1}{B}\right)+\frac{1}{B}\frac{\acute{m}}{\overline{m}}. \tag{15}$$

As mentioned before, q is the heat transfer per unit volume and

$$q=\frac{\dot{m}}{V}C_p\Delta T_t=\frac{\rho_1 u_1}{\frac{V}{A}}C_p\Delta T_t. \tag{16}$$

By linearizing Eq. (16), the heat transfer fluctuation can be expressed as

$$\frac{q'}{\overline{q}}=A\frac{T'_{t2}}{\overline{T}_{t2}}-B\frac{T'_{t1}}{\overline{T}_{t1}}+\frac{\rho'_1}{\overline{\rho}_1}+\frac{u'_1}{\overline{u}_1}, \tag{17-a}$$

in which

$$A = -\frac{\overline{T}_{t2}}{\overline{\overline{T}}_{t2} - \overline{\overline{T}}_{t1}}, \tag{17-b}$$

$$B = -\frac{\overline{T}_{t1}}{\overline{\overline{T}}_{t2} - \overline{\overline{T}}_{t1}}. \tag{17-c}$$

The stagnation temperature is defined as [55].

$$T_t = T\left(1 + \frac{\gamma - 1}{2}M^2\right) \tag{18}$$

Linearization of this relation yields

$$\frac{T'_t}{\overline{T}_t} = \frac{1}{1 + \frac{1}{2}(\gamma - 1)M^2}\left[\gamma\left(\frac{p'}{\gamma\overline{p}}\right) - \frac{\rho'}{\rho} + (\gamma - 1)\frac{Mu'}{c}\right]$$
$$= \frac{1}{1 + \frac{1}{2}(\gamma - 1)M^2}\left[(\gamma - 1)\left(\frac{p'}{\gamma\overline{p}}\right) - \frac{s'}{c_p} + (\gamma - 1)\frac{Mu'}{c}\right]. \tag{19}$$

Further, the cross-sectional variation in a choked nozzle is associated with [22].

$$\frac{A}{A^*} = \frac{1}{M}\left(\frac{2}{\gamma + 1}\left(1 + \frac{1}{2}(\gamma - 1)M^2\right)\right)^{\frac{\gamma+1}{2(\gamma-1)}} \exp\left[\left(-\frac{\Delta s}{R}\right)\left(1 - \frac{T}{T_t}\right)\right], \tag{20}$$

where A^* is the throat surface area and Δs is the entropy change. Through linearization of this equation and considering constant temperature in each part of the nozzle ($\Delta s' = 0$), it can readily be shown that $\frac{M'}{M} = 0$ [23]. This implies that [14].

$$\frac{u'}{c} - \frac{\gamma}{2}M\left(\frac{p'}{\gamma p}\right) + \frac{1}{2}M\frac{\rho'}{\rho} = 0. \tag{21}$$

For a choked nozzle without any shock waves, the following relation holds

$$P_1^+ + P_1^- - P_2^+ - P_2^- = 0. \tag{22}$$

Heat transfer modifies the Mach number at the outlet of a conduit with a constant cross section [55]. However, the variation of Mach number through a heat transferring conduit with variable area section (e.g. a nozzle) differs from that of a constant area conduit, traditionally presented by Rayleigh line [56]. Considering the nozzle geometry, inlet condition and the variation of the stagnation temperature, outlet Mach number can be found by an iterative method [56].

3. Dispersion and dissipation of the entropy waves

3.1. A compact nozzle

If the length of a nozzle becomes negligible compared to the acoustic and entropic wavelengths, the compact assumption is valid. This assumption is often used in the low frequency limit.

3.1.1. Hydrodynamic mechanisms

Turbulent mixing and boundaries interactions may disturb the flow and cause the decay of entropy waves [41,47]. These are highly complicated and problem dependent phenomena. In the current investigation, the net effect of these is represented by a decay coefficient (k_n) for the entropy wave attenuation. Thus,

$$\frac{\sigma_2}{\sigma_1} = 1 - k_n, \tag{23}$$

where σ_2 and σ_1 respectively denote the amplitude of the entropy wave ($\sigma = \frac{s'}{c_p}$) in the downstream and upstream sections of the nozzle throat. k_n depends on the nozzle geometry and fluid flow and should be exclusively determined for each nozzle and flow condition. Considering Eqs. (7), (13), (15) and assuming an adiabatic, i.e. $\overline{T}_{t1} = \overline{T}_{t2}$, compact nozzle, incorporating Eq. (23), result in the following expressions for the response of a subcritical nozzle to a dissipative incident entropy wave

$$P_1^- = \left(\frac{-M_1M_2k_n\left(1 + \frac{1}{2}(\gamma - 1)M_1^2\right) + \frac{M_1}{2}\left(M_1^2(1 - k_n) - M_2^2 - \frac{2k_n}{\gamma - 1}\right)}{(1 - M_1)\left[M_1\left(1 + \frac{1}{2}(\gamma - 1)M_2^2\right) + M_2\left(1 + \frac{1}{2}(\gamma - 1)M_1^2\right)\right]}\right)\sigma, \tag{24}$$

$$P_2^+ = \frac{M_2}{M_2 + 1}\left(\frac{-M_1k_n\left(1 + \frac{1}{2}(\gamma - 1)M_2^2\right) + \frac{M_1^2}{2}(1 - k_n) - \frac{M_2^2}{2} - \frac{k_n}{\gamma - 1}}{M_1\left(1 + \frac{1}{2}(\gamma - 1)M_2^2\right) + M_2\left(1 + \frac{1}{2}(\gamma - 1)M_1^2\right)}\right)\sigma. \tag{25}$$

Following Marble and Candel [14], in the derivation of Eqs. (24) and (25) the transmitted acoustic wave in the upstream section (P_1^+) and the upstream propagating component in the downstream section (P_2^-) are assumed to be zero. Combining Eqs. (7) and (21)–(23), and assuming compactness, the acoustic response of a supercritical nozzle to a dissipative entropy wave is expressed by

$$P_2^- = \frac{1}{4}\left(\frac{-M_1 + \frac{k_n}{2}(\gamma - 1)M_1M_2 - M_2(1 - k_n)}{1 + \frac{1}{2}(\gamma - 1)M_1}\right)\sigma, \tag{26}$$

$$P_2^+ = \frac{1}{4}\left(\frac{-\frac{k_n}{2}(\gamma - 1)M_2M_1 + M_2(1 - k_n) - M_1}{1 + \frac{1}{2}(\gamma - 1)M_1}\right)\sigma, \tag{27}$$

and, the reflected component takes the same form as that derived by Marble and Candel [14],

$$P_1^- = \frac{-\frac{M_1}{2}}{1 + \frac{1}{2}(\gamma - 1)M_1}\sigma. \tag{28}$$

3.2. Heat transfer

Heat transfer can leave a decaying effect on the incident entropy wave as convective wave. Once again, it is assumed that an entropy wave is incident upon a subcritical nozzle. As explained earlier, in such configuration $P_1^+ = P_2^- = 0$. Setting $\sigma_1 = \sigma$ and manipulating Eqs. (7), (15) and (19), for a subcritical nozzle reveals

$$\frac{1}{1 + \frac{1}{2}(\gamma - 1)M_1^2}\left[(\gamma - 1)(1 - M_1)P_1^- + \sigma\right] + \frac{\dot{Q}}{\overline{\dot{m}}C_p\overline{T}_{t1}} +$$
$$\left[-\left(1 + \frac{1}{B}\right)\frac{1}{1 + \frac{1}{2}(\gamma - 1)M_2^2}(\gamma - 1)(1 + M_2) - \frac{1}{B}\left(\frac{1}{M_2} + 1\right)\right]P_2^+ = \sigma_2\left(\frac{1 - \frac{B^{-1}}{2}(\gamma - 1)M_2^2}{\frac{1}{1 + \frac{1}{2}(\gamma - 1)M_2^2}}\right). \tag{29}$$

By applying Eq. (13) to the upstream and downstream sections of the nozzle and assuming zero unsteady heat transfer, a relation amongst the amplitudes of the transmission and reflection acoustic waves and that of the entropy wave is derived. This is

$$P_2^+ = \frac{M_2(M_1-1)}{M_1(M_2+1)}P_1^- - \frac{M_2}{M_2+1}\sigma + \frac{M_2}{M_2+1}\sigma_2. \tag{30}$$

Substituting Eq. (30) into (29) results in

$$\frac{K_{p1}}{K_{subc,\sigma 2}}P_1^- + \frac{K_{subc,\sigma}}{K_{subc,\sigma 2}}\sigma = \sigma_2, \tag{31-a}$$

where

$$K_{P1} = \frac{1}{1+\frac{1}{2}(\gamma-1)M_1^2}(\gamma-1)(1-M_1) - \left(1+\frac{1}{B}\right)\frac{1}{1+\frac{1}{2}(\gamma-1)M_2^2}(\gamma-1)\frac{M_2(M_1-1)}{M_1} - \frac{1}{B}\frac{(M_1-1)}{M_1}, \tag{31-b}$$

$$K_{subc,\sigma} = \frac{1}{1+\frac{1}{2}(\gamma-1)M_1^2} + \left(1+\frac{1}{B}\right)\frac{1}{1+\frac{1}{2}(\gamma-1)M_2^2}(\gamma-1)M_2 + \frac{1}{B}, \tag{31-c}$$

$$K_{subc,\sigma 2} = \frac{(1+B^{-1})((\gamma-1)M_2+1)}{1+\frac{1}{2}(\gamma-1)M_2^2}. \tag{31-d}$$

In Eq. (31-c) and (31-d), subscript "subc" denotes subcritical status. Due to the smaller length and flow residence time of the upstream part compared to those in the downstream section, it is assumed that heat transfer has a negligible effect on the convergent part. Considering this assumption, the reflected entropic wave is expressed by Ref. [14].

$$P_1^- = -\left(\frac{M_2-M_1}{1-M_1}\right)\left[\frac{\frac{1}{2}M_1\sigma}{1+\frac{1}{2}(\gamma-1)M_1M_2}\right]. \tag{32}$$

The ratio of the transmitted and incident entropy waves is defined as

$$\frac{\sigma_2}{\sigma} = \frac{K_{p1}}{K_{sub,\sigma 2}}\left(\frac{M_1-M_2}{1-M_1}\right)\left[\frac{\frac{1}{2}M_1}{1+\frac{1}{2}(\gamma-1)M_1M_2}\right] + \frac{K_\sigma}{K_{sub,\sigma 2}}. \tag{33}$$

By substituting this ratio into $k_n = 1 - \frac{\sigma_2}{\sigma}$ and Eq. (25), one can readily find the amplitude of the transmitted wave. In the supercritical case, P_1^-, $P_2^+$and P_2^- should be considered. By assuming negligible heat transfer effect on the upstream section of the nozzle, the reflected entropy wave becomes the same as Eq. (28). Using Eq. (7),

$$\rho_2^+ = P_2^+ - \sigma_2. \tag{34}$$

Eq. (18) then provides the transmission wave,

$$P_2^+ = P_2^-\left(\frac{1+\frac{1}{2}(\gamma-1)M_2}{1-\frac{1}{2}(\gamma-1)M_2}\right) + \frac{\sigma_2}{2}\left(\frac{M_2}{1-\frac{1}{2}(\gamma-1)M_2}\right). \tag{35}$$

By using Eq. (22) and after some algebraic manipulation, it can be shown that

$$P_2^+ = -\frac{M_1}{4}\left(\frac{1+\frac{1}{2}(\gamma-1)M_2}{1+\frac{1}{2}(\gamma-1)M_2}\right)\sigma + \frac{M_2}{4}\sigma_2. \tag{36}$$

Combining Eqs. (15) and (22) yields the following equation

$$\left(\frac{1+\frac{1}{2}(\gamma-1)M_2^2}{1-\frac{B^{-1}}{2}(\gamma-1)M_2^2}\right)\left(\frac{1}{1+\frac{1}{2}(\gamma-1)M_1^2}(\gamma-1)(1-M_1) - \frac{1}{1+\frac{1}{2}(\gamma-1)M_2^2}\left(1+B^{-1}\right)(\gamma-1)(1-M_2) - B^{-1}\left(1-\frac{1}{M_2}\right)\right)$$
$$P_1^- + \frac{1}{1+\frac{1}{2}(\gamma-1)M_1^2}\left(\frac{1+\frac{1}{2}(\gamma-1)M_2^2}{1-\frac{B^{-1}}{2}(\gamma-1)M_2^2}\right)\sigma - \left(\frac{1+\frac{1}{2}(\gamma-1)M_2^2}{1-\frac{B^{-1}}{2}(\gamma-1)M_2^2}\right)\left(\frac{2M_2(\gamma-1)\left(1+B^{-1}\right)}{1+\frac{1}{2}(\gamma-1)M_2^2} + \frac{2B^{-1}}{M_2}\right) \tag{37}$$
$$P_2^+ = \sigma_2 - \frac{\dot{Q}}{\overline{\dot{m}}C_p\overline{T}_{t1}}\left(\frac{1+\frac{1}{2}(\gamma-1)M_2^2}{1-\frac{B^{-1}}{2}(\gamma-1)M_2^2}\right).$$

Considering Eqs. ((22), (28), (36) and (37), the ratio of the incident and transmitted entropy waves becomes

$$\frac{\sigma_2}{\sigma} = \frac{K_{supc,\sigma}}{K_{supc,\sigma 2}}, \tag{38-a}$$

where

$$K_{supc,\sigma}=\left(\frac{1+\frac{1}{2}(\gamma-1)M_2^2}{1-\frac{B^{-1}}{2}(\gamma-1)M_2^2}\right)\left(\frac{-\frac{M_1}{2}}{1+\frac{1}{2}(\gamma-1)M_1}\left(\frac{(\gamma-1)(1-M_1)}{1+\frac{1}{2}(\gamma-1)M_1^2}-\frac{(1+B^{-1})(\gamma-1)(1-M_2)}{1+\frac{1}{2}(\gamma-1)M_2^2}-B^{-1}\left(1-\frac{1}{M_2}\right)\right)+\frac{1}{1+\frac{1}{2}(\gamma-1)M_1^2}\right)+$$
$$\left(\frac{1+\frac{1}{2}(\gamma-1)M_2^2}{1-\frac{B^{-1}}{2}(\gamma-1)M_2^2}\right)\left(\frac{2M_2(\gamma-1)\left(1+B^{-1}\right)}{1+\frac{1}{2}(\gamma-1)M_2^2}+2B^{-1}\right), \tag{38-b}$$

$$K_{supc,\sigma 2}=1+\frac{M_2}{4}\left(\frac{1+\frac{1}{2}(\gamma-1)M_2^2}{1-\frac{B^{-1}}{2}(\gamma-1)M_2^2}\right)\left(\frac{2M_2(\gamma-1)(1+B^{-1})}{1+\frac{1}{2}(\gamma-1)M_2^2}+\frac{2B^{-1}}{M_2}\right), \tag{38-c}$$

and subscript "supc" stands for the supercritical condition. P_2^+ and P_2^- are obtained by Eqs. (26) and (27). Further, P_1^- is found through Eq. (22). Here, the response of heat transferring nozzle to an incident acoustic wave by the strength of ${P_1}^+=\varepsilon$ is further analysed. Considering Eqs. (12) and (13), in the subcritical regime, a relation amongst the transmitted acoustic wave in the diverging part and the acoustic components in the converging section is derived. This is

$${P_2}^+=\frac{1}{M_1(1+M_2)}\left[M_2\left({P_1}^+-{P_1}^-\right)+M_1M_2\left({P_1}^++{P_1}^-\right)\right]. \tag{39}$$

Combining Eqs. (12), (17) and (19) gives

$${P_1}^-=\frac{{K_1}^+}{{K_1}^-}\varepsilon, \tag{40-a}$$

where

$${K_1}^+=-B\left(1+\frac{1}{2}(\gamma-1){M_2}^2\right)(\gamma-1)(1+M_1)+A\left(1+\frac{1}{2}(\gamma-1){M_1}^2\right)(\gamma-1)\left(\frac{M_2}{M_1}+M_2\right)+\left(1+\frac{1}{2}(\gamma-1){M_1}^2\right)\left(1+\frac{1}{2}(\gamma-1){M_2}^2\right)\left(\frac{-(\gamma M_2+1)}{M_1(1+M_2)}-\frac{(\gamma M_2+1)}{(1+M_2)}+(\gamma-1)\right), \tag{40-b}$$

$${K_1}^-=B\left(1+\frac{1}{2}(\gamma-1){M_2}^2\right)(\gamma-1)(1-M_1)+A\left(1+\frac{1}{2}(\gamma-1){M_1}^2\right)(\gamma-1)\left(\frac{M_2}{M_1}-M_2\right)+\left(1+\frac{1}{2}(\gamma-1){M_1}^2\right)\left(1+\frac{1}{2}(\gamma-1){M_2}^2\right)\left(\frac{(\gamma M_2+1)}{(1+M_2)}-\frac{(\gamma M_2+1)}{M_1(1+M_2)}+(\gamma-1)\right). \tag{40-c}$$

The transmitted acoustic wave in the downstream section is found by substituting Eq. (40-a) into Eq. (39), which gives

$$P_2^+=\frac{1}{M_1(1+M_2)}\left[M_2\varepsilon\left(1-\frac{K_1^+}{K_1^-}\right)+M_1M_2\varepsilon\left(1+\frac{K_1^+}{K_1^-}\right)\right]. \tag{41}$$

In the supercritical regime, relations derived by Marble and Candel [14] are still valid. These are

$${P_1}^-=\frac{1-\frac{1}{2}(\gamma-1)M_1}{1+\frac{1}{2}(\gamma-1)M_1}\varepsilon, \tag{42}$$

$${P_2}^+=\frac{1+\frac{1}{2}(\gamma-1)M_2}{1+\frac{1}{2}(\gamma-1)M_1}\varepsilon, \tag{43}$$

$${P_2}^-=\frac{1-\frac{1}{2}(\gamma-1)M_2}{1+\frac{1}{2}(\gamma-1)M_1}\varepsilon. \tag{44}$$

However, the outlet Mach number should be now calculated by the iterative method [56] which involves heat transfer effect.

3.2.1. Combined effects of hydrodynamic mechanisms and heat transfer

The analyses presented in sections 3.1.1 and 3.1.2 are linear and therefore, the principle of superposition holds. Hence,

$$\sigma_{2,\text{with heat transfer,no dissipation}}=\sigma_{2\text{with heat transfer,with dissipation}}+k_n\sigma.$$

Accordingly, through using Eq. (33) for a subcritical nozzle, it can be shown that

$$\frac{\sigma_2}{\sigma}=\frac{1}{K_{subc,\sigma 2}}\left(K_{P1}\left(\frac{M_1-M_2}{1-M_1}\right)\frac{\frac{1}{2}M_1}{1+\frac{1}{2}(\gamma-1)M_1M_2}+K_{subc,\sigma}\right)-k_n, \tag{45}$$

while P_2^+ is found by substituting Eq. (45) into Eq. (25). In the supercritical regime, using Eq. (38),

$$\frac{\sigma_2}{\sigma}=\frac{K_{supc,\sigma}}{K_{supc,\sigma 2}}-k_n, \tag{46}$$

and P_2^+ and P_2^- are calculate by Eqs. (26) and (27), respectively.

3.3. Non-compact nozzle

3.3.1. Stretch of the entropy wave in the nozzle

As stated earlier, so far, there has been no attempt for calculating the stretch of a convective front in a nozzle. This section considers

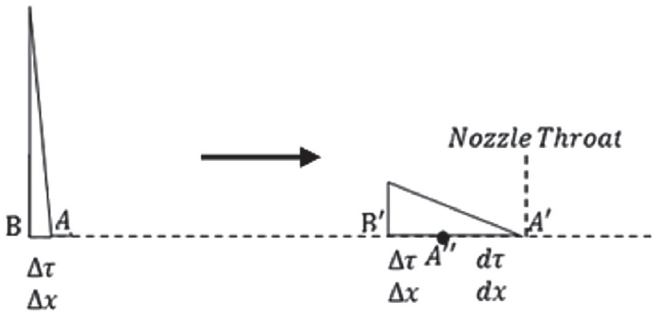

Fig. 2. Motion of the entropy wave from inlet to the nozzle throat.

the stretch of entropy wave as it convects through the nozzle from the inlet to the throat. In the current problem, the kinematic acceleration of the convective flow is the main cause of the wave stretch. The flow acceleration is not spatially constant, however, a mean value of acceleration is utilised here. The motion of the entropy wave is illustrated in Fig. 2. This configuration is chosen on the basis the analysis in Ref. [41].

In Fig. 2, $\Delta\tau$ and $d\tau$ are respectively the temporal wave width and stretch of the incident entropy wave in the time domain and $\Delta\tau' = \Delta\tau + d\tau$. Further, it is assumed that the distance between A and B at the inlet approaches zero. Utilising simple kinematic relations reveals the following relation for the temporal width of the entropy wave at the throat

$$\Delta\tau' = \frac{V^* - \sqrt{2aV_0\Delta\tau - 2aV^*\Delta\tau + V^{*2}}}{a} \tag{47}$$

where V_0, V^* and a are the velocity at the inlet, velocity at the throat and mean acceleration, respectively. To obtain the transfer function of the convected entropy wave from the inlet to the throat, an approach similar to that of Ref. [38] is taken. The wave function between the throat and the inlet may be related by a Green function. That is

$$\sigma_2 = \int_0^t G(t)\sigma_{inlet}(t-\tau)d\tau, \tag{48}$$

in which, τ is the convection time of a flow particle from the inlet to the throat. If the Green function is known, the final function will be calculated by the integration of Eq. (48). Using Laplace transformation, the integration is transformed to

$$\sigma_2(s) = G(s)\sigma_1(s). \tag{49}$$

According to the primary assumption of the extreme vicinity of A and B, the incident wave can be assumed to be an impulse (Dirac delta function). In other word, $\sigma_1(t) = \delta(t)$. Hence, $\sigma_1(s) = 1$ and the final wave function becomes identical to the Green function. That is

$$\sigma_2(s) = G(s). \tag{50}$$

Considering energy balance for the entropy wave,

$$(1-k_n)\int_{-\infty}^{+\infty}\sigma_{inlet}dt = (1-k_n)\int_{-\infty}^{+\infty}\delta(t)dt = \int_{-\infty}^{+\infty}\sigma_2 dt = \sigma_{final}\Delta\tau^{"}, \tag{51}$$

where σ_{final} is the amplitude of the entropy wave (or size of the vertical side of the triangle) in the final wave configuration. Further, $\Delta\tau^{"} = \Delta\tau'/2$ and therfore

$$\sigma_{final} = \frac{1-k_n}{\Delta\tau^{"}}. \tag{52}$$

Furthermore,

$$\sigma_2 = \frac{-\sigma_{final}}{2\Delta\tau^{"}}\left(t - (\tau + \Delta\tau^{"})\right) \quad \tau - \Delta\tau^{"} < t < \tau + \Delta\tau^{"}. \tag{53}$$

Finally, a transfer function is calculated by applying the Fourier transformation,

$$G(i\omega) = \frac{1-k_n}{2\omega^2\Delta\tau^{"2}}e^{-i\omega\tau}\left(e^{i\omega\Delta\tau^{"}}(1-2\Delta\tau^{"}i\omega) - e^{-i\omega\Delta\tau^{"}}\right), \tag{54}$$

which provides the amplitude and phase of the stretched wave at the throat. To study the stretch effects only, k_n in Eq. (54) should be set to zero.

3.4. Effective length of a nozzle with heat transfer

This section extends the analysis of non-adiabatic flow to non-compact nozzles. Similar to Ref. [18], the concept of "Effective Length" is utilised here. Effective length approximates a nozzle with two connected conduits without any change in the cross-sectional area (Fig. 3). Each conduit has its own length as an effective length.

To find the effective length, the linearized equations of mass, momentum and energy (Eq. (4), (5) and (6)) are considered. Dimensionless flow perturbations may be written as

$$\frac{p'}{\gamma\bar{p}} = \hat{p}(X)e^{i\omega t}, \quad \frac{\rho'}{\bar{\rho}} = \hat{\rho}(X)e^{i\omega t}, \quad \frac{u'}{\bar{u}} = \hat{u}(X)e^{i\omega t}, \tag{55}$$

in which X = x/L and L is the axial nozzle length.

3.5. Asymptotic analysis of a supercritical nozzle

In a choked nozzle, Mach number and the dimensionless frequency may be presented with respect to the flow velocity at the

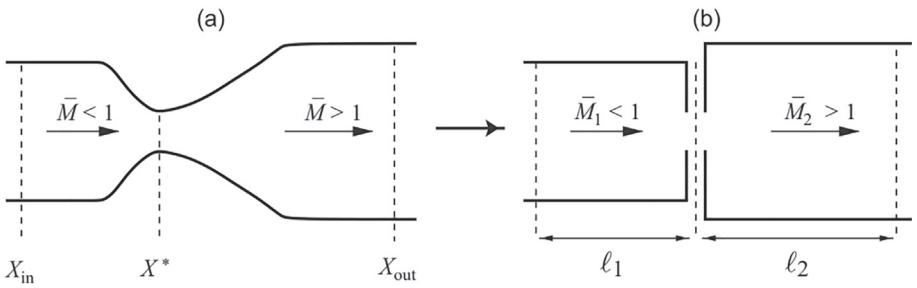

Fig. 3. (a) A convergent-divergent nozzle (b) Equivalent conduits of constant cross-sectional areas.

throat (i.e. sonic speed c). Thus,

$$M^* = \frac{\overline{u}}{c^*}, \quad \Omega = \frac{\omega L}{c^*},$$

in which, the superscript * denotes the throat of a choked nozzle and Ω is the dimensionless frequency and L stands for the axial length of the nozzle. After removing the steady flow component and using the dimensionless perturbations, the mass conservation equation is written as [18].

$$i\Omega\hat{\rho} + M^*\left(\frac{d\hat{u}}{dX} + \frac{d\hat{\rho}}{dX}\right) = 0. \tag{56}$$

The energy equation reduces to

$$i\Omega\left(\hat{p} - \hat{\rho}\right) + M^*\left(\frac{d\hat{p}}{dX} + \frac{d\hat{\rho}}{dX}\right) = M^*\frac{\Delta T_t}{\overline{T}}\left(\hat{q} - \hat{p} - \hat{u}\right). \tag{57}$$

Conservation of the total enthalpy in the mean flow results in

$$\overline{c}^2 = \frac{c^{*2}}{2}(\gamma+1) - \frac{\overline{u}^2}{2}(\gamma+1) + \overline{Q}(\gamma-1). \tag{58}$$

It should be noted that the unit of $\overline{q}$ in Eq. (3) is W/m^3. However, the unit of $\overline{Q}$ in Eq. (58) is J/kg. Thus,

$$\overline{Q} = \overline{q}\frac{V}{\dot{m}} = c_p\Delta T_t. \tag{59}$$

By employing Eqs. (50) and (51), the momentum equation becomes

$$i\Omega\hat{u} + M^*\frac{d\hat{u}}{dX} + \frac{dM^*}{dX}\left(2\hat{u} + \hat{\rho} - \gamma\hat{p}\right) + \frac{1}{2}\frac{d\hat{p}}{dX}\left[\frac{\gamma+1}{M^*} - (\gamma-1)M^* + \frac{2c_p\Delta T_t}{M^*c^{*2}}(\gamma-1)\right] = 0. \tag{60}$$

Further, an algebraic manipulation of Eqs. (49), (52) and (58) reveals

$$i\Omega\left[M^*\left(2\hat{u} + \hat{\rho} - \hat{p}\right) - \frac{1}{M^*}\left(\hat{\rho} + \hat{p}\right)\right] + \frac{d}{dX}\left[(M^{*2}-1)\left(2\hat{u} + \hat{\rho} - \gamma\hat{p}\right)\right] + \frac{d\hat{p}}{dX}\frac{2c_p\Delta T_t}{c^{*2}}(\gamma-1) + (M^{*2}-1)\frac{\Delta T_t}{\overline{T}}\left(\hat{q} - \hat{p} - \hat{u}\right) = 0. \tag{61}$$

Flow perturbations may be presented by the following asymptotic expansions [18].

$$\hat{p} = \hat{p}_0 + i\Omega\hat{p}_1 + O\left(\Omega^2\right), \tag{62-a}$$

$$\hat{\rho} = \hat{\rho}_0 + i\Omega\hat{\rho}_1 + O\left(\Omega^2\right), \tag{62-b}$$

$$\hat{u} = \hat{u}_0 + i\Omega\hat{u}_1 + O\left(\Omega^2\right). \tag{62-c}$$

By substituting Eq. (62) into Eq. (61), the boundary conditions of a choked nozzle for the zeroth order are derived. These are

$$2\hat{u}_0 + \hat{\rho}_0 - \gamma\hat{p}_0 = 0, \tag{63}$$

$$\hat{q}_0 - \hat{u}_0 - \hat{p}_0 = 0. \tag{64}$$

Due to neglecting the higher order terms, Eqs. (63) and (64) are valid for a compact nozzle. Eq. (63) was derived by Stow et al. [17] and later by Goh and Morgans [18]. It is noted that Eq. (64) is essentially the same as Eq. (12).

The first order of asymptotic expansion of Eq. (61) is integrated. This reveals

$$\left[\left(M^{*2}-1\right)\left(2\hat{u}_1 + \hat{\rho}_1 - \hat{p}_1\right)\right]_{X_1}^{X_2} = \left(\hat{\rho}_0 + \hat{p}_0\right)\int_{X_1}^{X_2}\frac{dX}{M^*} - \left(2\hat{u}_0 + \hat{\rho}_0 - \hat{p}_0\right)\int_{X_1}^{X_2}M^*dX - 2(\gamma-1)c_p\Delta T_t\int_{X_1}^{X_2}\frac{M^{*2}}{\overline{u}^2}d\hat{p}_1 - \int_{X_1}^{X_2}\frac{\Delta T_t}{\overline{T}}(M^{*2}+1)\left(\hat{q}_1 - \hat{p}_1 - \hat{u}_1\right)dX. \tag{65}$$

By using Eq. (65) in the range of $X = X_{in}$ to $X = X^*$ and consideration of $\overline{c} = \sqrt{\gamma R\overline{T}}$ and $\frac{c_p}{\gamma R}(\gamma - 1) = 1$, the effective length of the convergent part is found as follows

$$l_1 = \int_{X_{in}}^{X^*}\frac{\overline{M}_0}{\overline{M}}\sqrt{\frac{1 + \frac{\gamma-1}{2}\overline{M}^2 - \frac{\Delta T_{t1}}{\overline{T}}}{1 + \frac{\gamma-1}{2}\overline{M}_0^2 - \frac{\Delta T_{t1}}{\overline{T}_1}}}dX, \tag{66}$$

in which $\overline{M}_0$ and $\overline{T}_1$ are respectively the mean inlet Mach number and temperature and $\Delta T_{t1} = T^* - T_{t1}$. It should be noted that due to the assumption of $M^* \ll 1$ in deriving Eq. (65), the terms including the multiplication of M^* can be neglected before those including $1/M^*$.

For the divergent part, Eq. (65) should be implemented between $X = X^*$ and $X = X_{out}$. In accordance with Eq. (63), the effective length of the divergent part is obtained as

$$l_2 = \frac{\left(\hat{p}_0 + \hat{\rho}_0\right)\int_{X_{in}}^{X^*}\frac{1}{M^*}dX - (\gamma-1)\hat{p}_0\int_{X_{in}}^{X^*}M^*dX}{\frac{\left(\hat{p}_0 + \hat{\rho}_0\right)}{M_2^*} - (\gamma-1)\hat{p}_0M_2^*}, \tag{67}$$

where M_2^* is the outlet Mach number, which can be rewritten in accordance with the first law of thermodynamics,

$$M_2^* = \sqrt{\frac{\frac{\gamma+1}{2}}{1 + \frac{\gamma-1}{2}\overline{M}^2 - \frac{\Delta T_{t2}}{\overline{T}_2}}}. \tag{68}$$

Duran and Moreaue [26] showed that indirect noise prevails only at low frequencies. Hence, to assess the entropy noise, the values of $\hat{p}_0 + \hat{\rho}_0$ and $\hat{p}_0$ are substituted from the results of the compact nozzle in section of 3.1.3. These present the combined effects of heat transfer and hydrodynamic mechanisms. The other important note is that for a nozzle with an incident acoustic wave, the acoustic part of $\hat{\rho}_0$ should be used (this means $\hat{\rho}_0 = \hat{p}_0$) in Eq. (67). As a result, the acoustic effective length ($l_{2,p}$) and entropic effective length ($l_{2,\sigma}$) are different in the convergent and divergent parts. The acoustic phase response of the nozzle to an incident

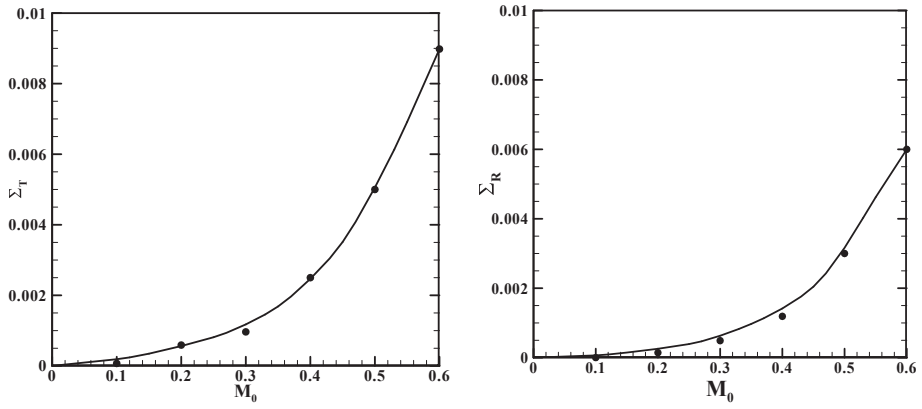

Fig. 4. The acoustic energy reflection (a) and transmission coefficient (b) to an incident entropic wave. The current relations (solid line) and the numerical simulation of Ref. [52] (dots).

entropy wave, σ, for the first order of Ω may be expressed as [18].

$$\frac{P_2^+}{\sigma}=\left|\frac{P_2^+}{\sigma}\right|e^{ik_2^+l_{2,\sigma}+ik_0^+l_1}+O\left(\Omega^2\right), \tag{69}$$

$$\frac{P_2^-}{\sigma}=\left|\frac{P_2^-}{\sigma}\right|e^{ik_2^-l_{2,\sigma}+ik_0^+l_1}+O\left(\Omega^2\right), \tag{70}$$

where $k_2^+ = \omega/(\bar{c}_2+\bar{u}_2)$, $k_2^- = \omega/(\bar{c}_2-\bar{u}_2)$ and $k_0^+ = \omega/\bar{u}_1$. Similarly, the nozzle responses to acoustic waves are [18].

$$\frac{P_2^+}{P_1^+}=\left|\frac{P_2^+}{P_1^+}\right|e^{ik_2^+l_{2,p}+ik_1^+l_1}+O\left(\Omega^2\right), \tag{71}$$

$$\frac{P_2^-}{P_1^+}=\left|\frac{P_2^-}{P_1^+}\right|e^{ik_2^-l_{2,p}+ik_1^+l_1}+O\left(\Omega^2\right), \tag{72}$$

in which $k_1^+ = \frac{\omega}{\bar{c}_1+\bar{u}_1}$.

4. Combustion of the lean premixed mixture

Lean-premixed mixtures of pure hydrogen and air can react at an equivalence ratio as low as 0.14 [57] with a combustion reaction given by

$$H_2+3.57(O_2+3.76N_2)\rightarrow H_2O+3.07O_2+13.42N_2 \tag{73}$$

The heat capacity of the working fluid (the mixture of O_2, H_2O and N_2) are calculated on the basis of their mole fractions using Dalton model [58].

5. Validation

It is noted that currently there is no publicly available experimental data for comparison against the developed analytical model. Therefore, the analytical results are compared with the published numerical results and the existing theoretical results in the limit of no wave decay. To demonstrate the validity of the relations derived in Section 3, the following two main points are considered. (1) When variation of the stagnation temperature tends to zero (i.e. flow becomes adiabatic), the values of A and B in Eq. (17) approach infinity. Under this condition, Eqs. (24) to (27), (30), (31), (36), (39), (40-a) and (46) reduce to those of Marble and Candel [14]. Further, the relations of effective length, Eqs. (66) and (67), reduce to those of Goh and Morgans [18]. Moreover, by setting the dissipation of entropy waves to zero, Eqs. (33) and (38) tend to unity, which means $\sigma_2=\sigma_1$, i.e. as expected, the entropy wave remains unchanged. Furthermore, expectedly, by setting $\omega=0$, the transfer function G in Eq. (54) tends to unity. This means that in the limit of zero frequency there is no dispersion of the entropy waves, which is consistent with the physics of the problem.

(2) Karimi et al. [51,52] calculated the acoustic energy of reflection (Σ_R) and transmission (Σ_T) coefficient in a duct with a mean temperature gradient. In their setting, the incident wave was entropic (σ), and they defined acoustic energy reflection and transmission coefficients as [51].

$$\Sigma_R=\frac{(\gamma-1)(1-\overline{M}_0)^2}{\bar{\rho}_0^2\overline{M}_0\bar{c}_0^4}\left|\frac{R}{\sigma}\right|^2,\quad \Sigma_T=\frac{(\gamma-1)(1+\overline{M}_l)^2}{\bar{\rho}_0\bar{\rho}_l\overline{M}_0\bar{c}_0\bar{c}_l}\left|\frac{T}{\sigma}\right|^2, \tag{74}$$

where R and T are the reflected and transmitted components of the acoustic wave [51,52]. Under compact conditions, these coefficients were calculated by the current relations and compared by the low

Table 1
The inlet and outlet Mach numbers and area ratios of the adiabatic nozzle from Ref. [23].

		Unchoked	Choked
		$M_2 = 0.4$	$M_2 = 1.2$
M_1=0.025	A_1/A^*	14.604	23.365
	A_2/A^*	1.000	1.032
M_1=0.05	A_1/A^*	7.310	11.695
	A_2/A^*	1.000	1.032
M_1=0.1	A_1/A^*	3.671	5.873
	A_2/A^*	1.000	1.032

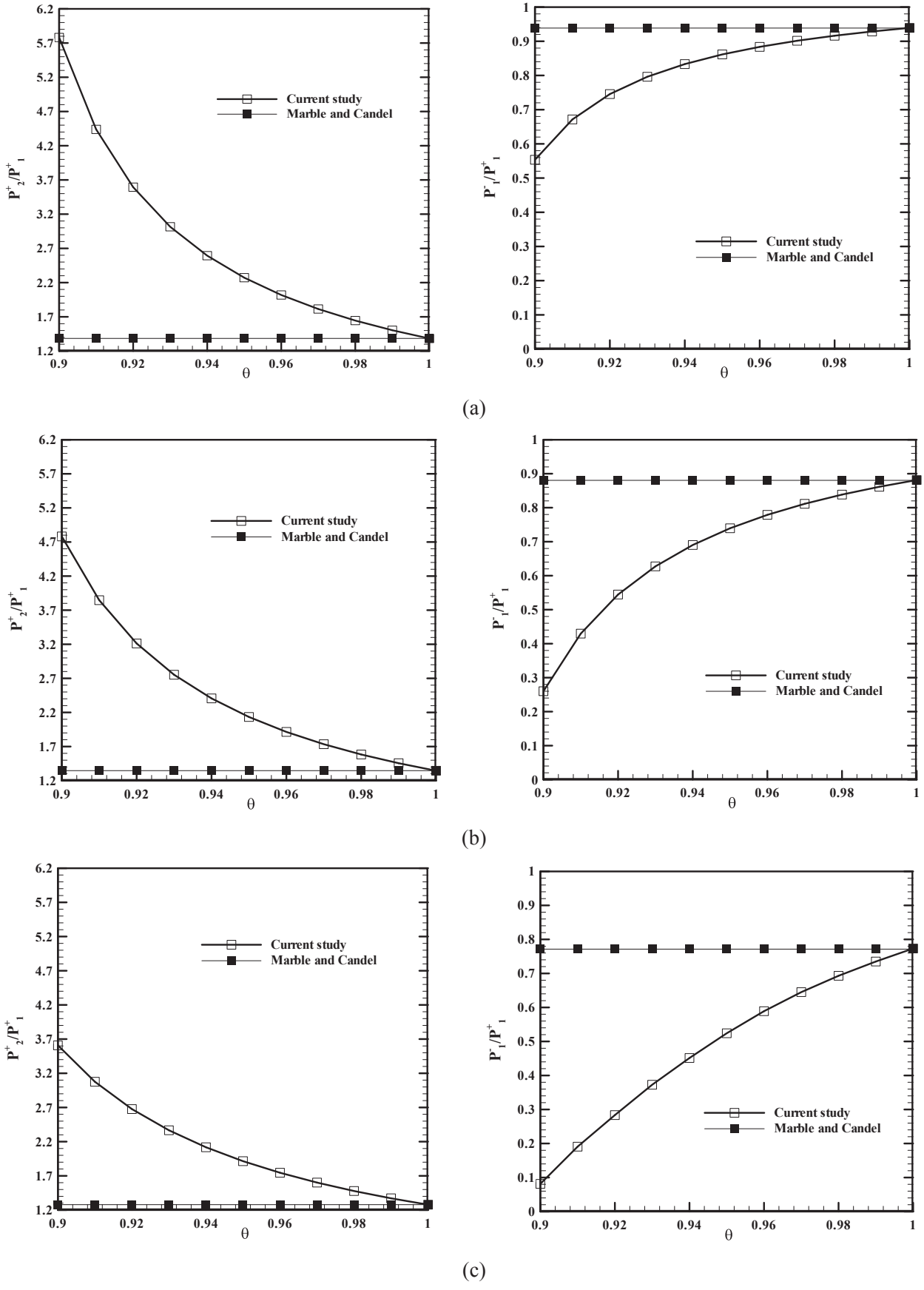

Fig. 5. Transmitted and reflected acoustic waves (P_1^- and P_2^+) in a subcritical nozzle subject to an incident acoustic wave (P_1^+) for the inlet Mach number of (a) 0.025, (b) 0.05 and (c) 0.1.

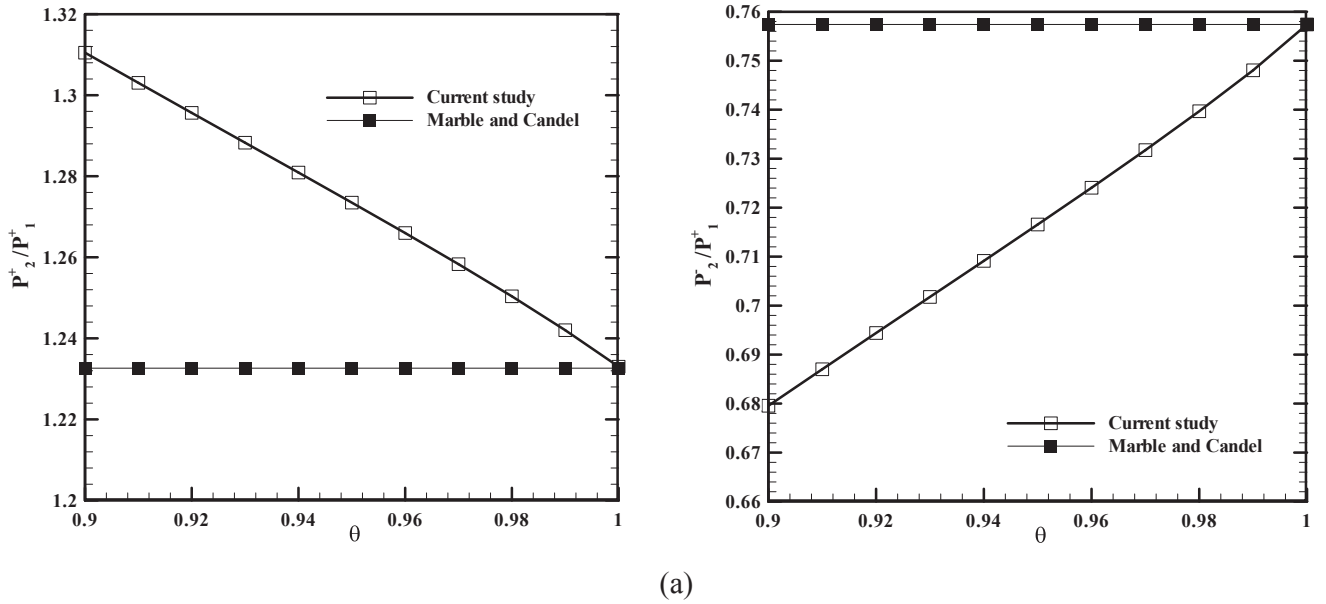

(a)

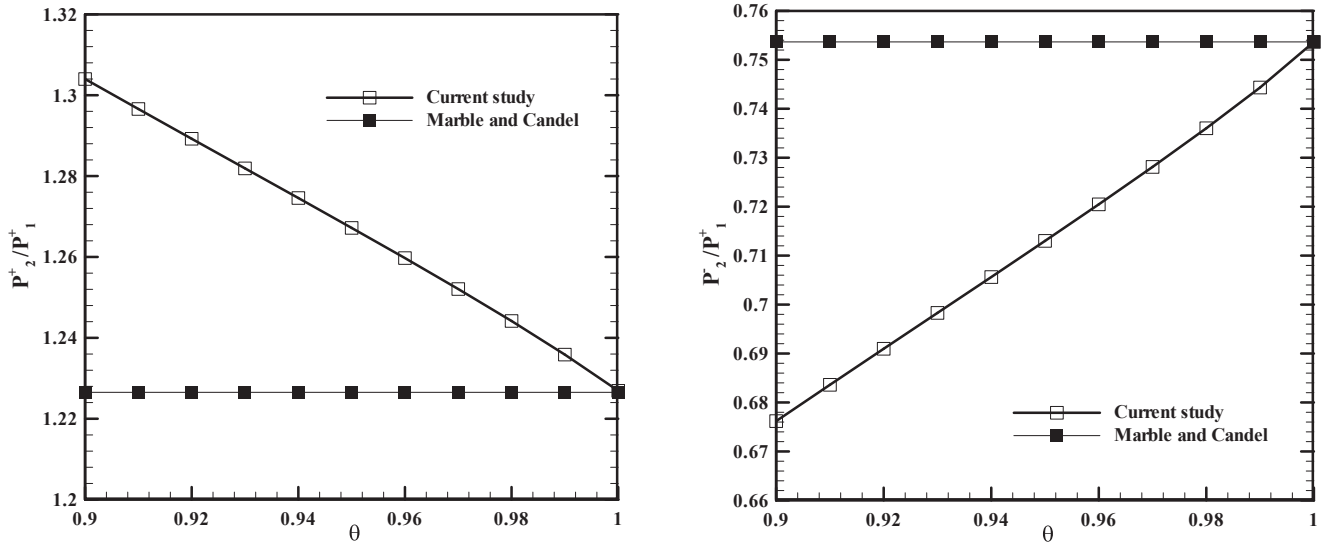

(b)

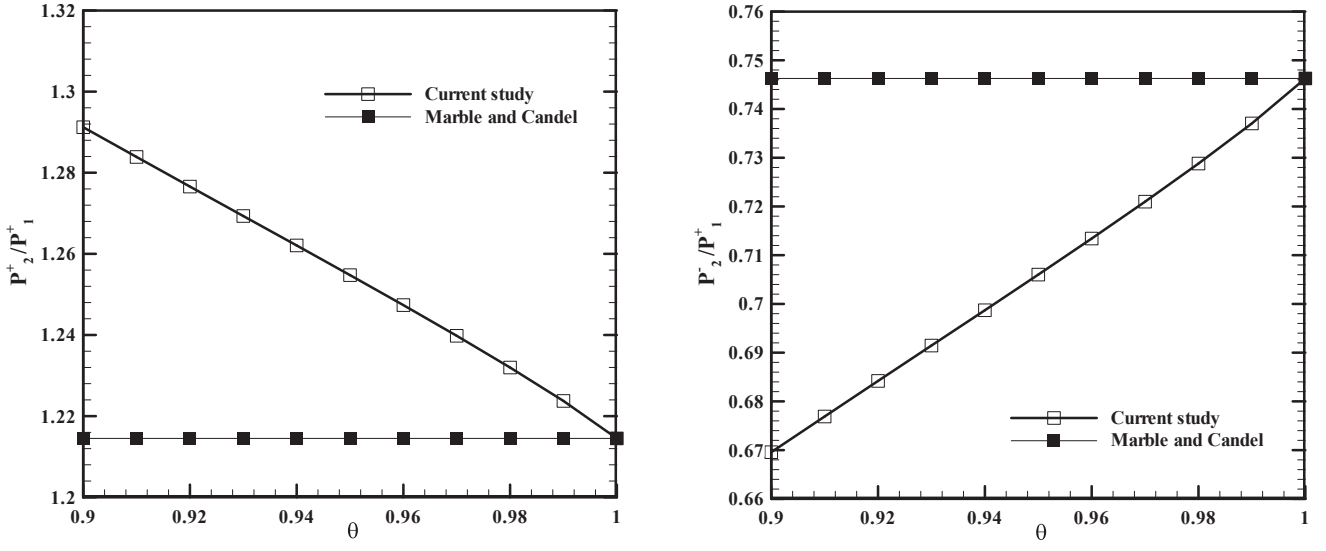

(c)

Fig. 6. Amplitudes of the transmitted acoustic waves (P_2^- and P_2^+) in a supercritical nozzle subject to an incident acoustic wave (P_1^+) for the inlet Mach number of (a) 0.025, (b) 0.05 and (c) 0.1.

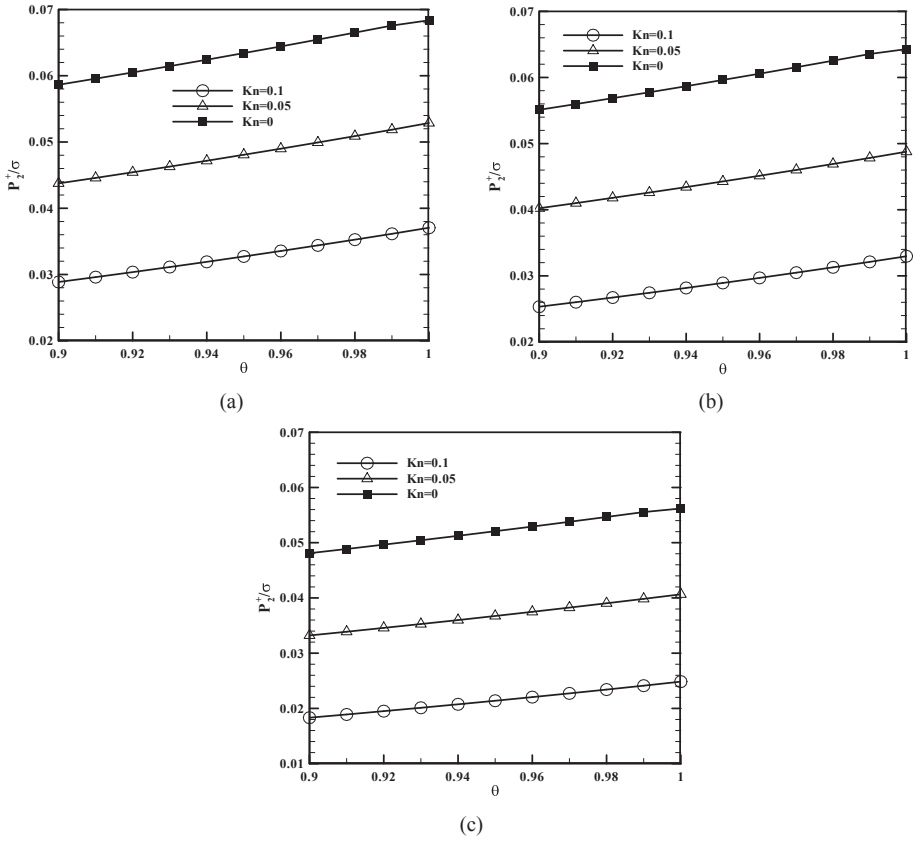

Fig. 7. Transmitted acoustic wave (P_2^+) for a subcritical nozzle subject to an incident entropy wave (σ) for varying inlet Mach numbers (a) 0.025 (b) 0.05 (c) 0.1.

frequency simulation of Karimi et al. [52], in which $\frac{T_{t2}}{T_{t1}} = 0.5$. Fig. 4 depicts this comparison, which shows an excellent agreement.

These two series of evidence serve as the validation of the current theoretical work.

It should be noted that the analysis for predicting noise amplitude was based on compact nozzle, which implies zero frequency. Nonetheless, compact nozzle assumption can be well utilised for the evaluation of finite frequency noise [21,22,48] (e.g. rumble [34,47]) with an acceptable accuracy depending on the flow conditions [21,22]. Due to the use of 'effective length', prediction of the phase shift is independent of the frequency. Further, the valid range for Mach number is $M < 1$ for subcritical conditions and $M > 1$ for supercritical nozzle.

6. Results and discussions

6.1. The nozzle geometry

In the current work, the divergent section of the nozzle is ten times longer than that of the convergent section. The area ratio is chosen such that the outlet Mach numbers do not change in the selected inlet Mach numbers, as Table 1 illustrates [23].

6.2. Heat transfer and hydrodynamic mechanisms in compact nozzles

Fig. 5 shows the amplitudes of the reflected and transmitted waves in a compact, heat transferring nozzle subject to an incident acoustic wave. The horizontal axis in this figure represents the nozzle outlet to inlet stagnation temperature ratio (θ). This figure also contains the results of Marble and Candel [14], which are independent of the variations in the stagnation temperature and assume an adiabatic flow. Fig. 5 illustrates transmitted and reflected noise in a subcritical nozzle of various Mach numbers. This figure clearly shows that for the considered Mach numbers, intensification of the cooling rate (decreasing θ) results in increasing the amplitude of the transmitted wave and decreasing that of the reflected wave. Importantly, as the ratio of the outlet to inlet stagnation temperature approaches unity, the amplitudes of

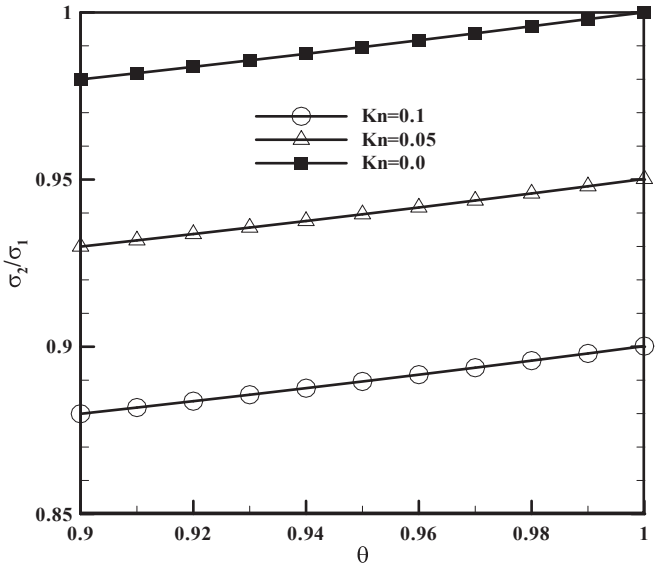

Fig. 8. Ratio of the outlet to inlet entropy waves (σ_2/σ_1) in a subcritical nozzle.

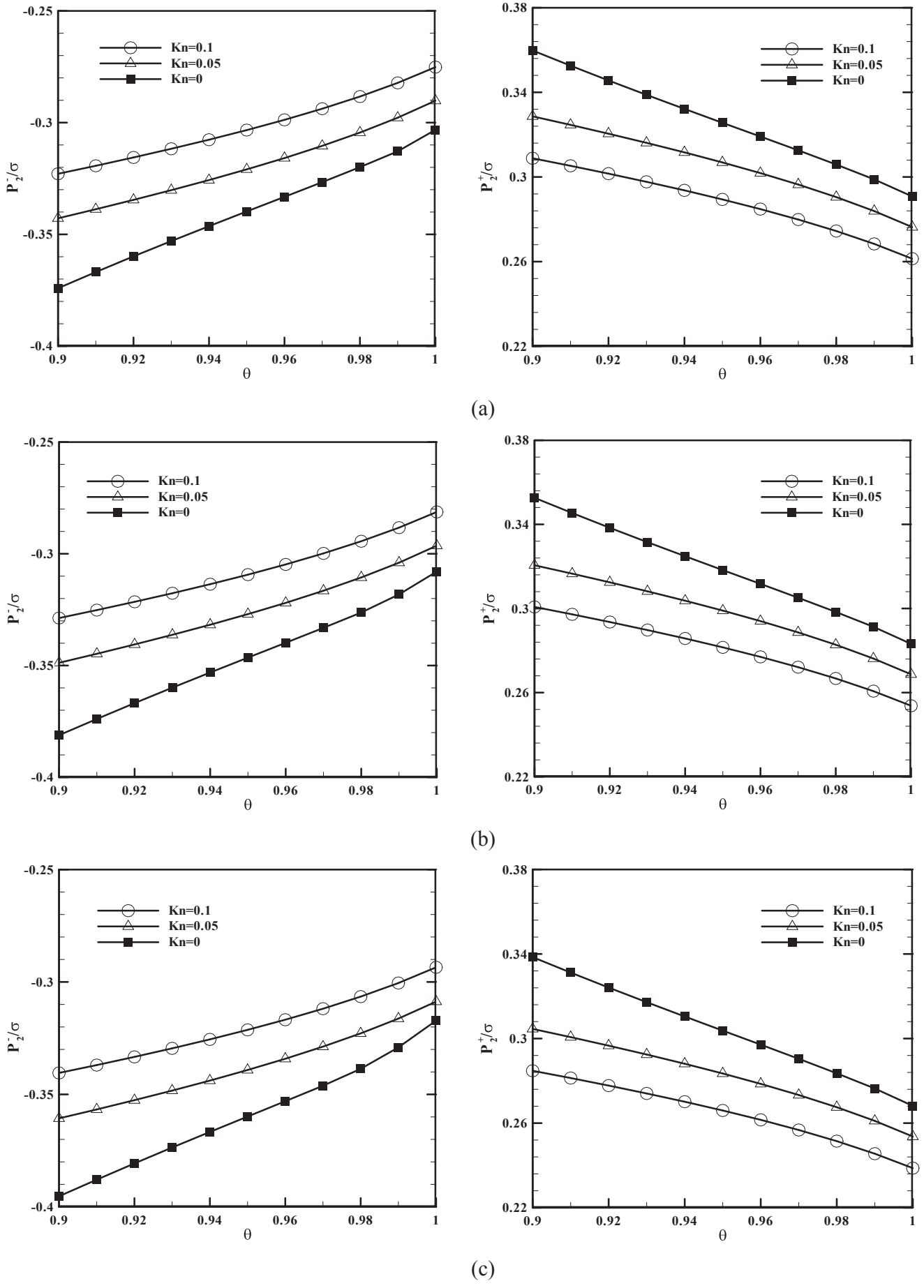

Fig. 9. Amplitude of the transmitted waves (P_2^+ and P_2^-) for a supercritical nozzle subject to an incident entropy wave (σ) for different inlet Mach numbers (a) 0.025 (b) 0.05 (c) 0.1.

both reflected and transmitted waves approach the values predicted by Marble and Candel [14] in an adiabatic flow.

Fig. 6 depicts the similar information as Fig. 5 for the corresponding supercritical nozzle. This figure shows that by intensifying the cooling rate in the supercritical nozzle, the amplitude of the P_2^+ increases, while that of P_2^- wave decreases. This trend is in agreement with the numerical results of Karimi et al. [53,54] for heat transferring flows in ducts with constant and variable cross-sections. Unlike the subcritical condition, the P_2^+ increment roams only around 6 to 7%. Further, the amplitude of the P_2^+ waves are smaller than those under the subcritical condition. In this case, the reduction in the amplitude of P_2^-waves is less than 10%. The response exhibits a linear behaviour in all investigated cases and for the adiabatic nozzle, the results coincide with those of Ref. [14].

Next, we analyse the influences of hydrodynamic mechanisms and heat transfer on the nozzle response. Fig. 7 shows the response of a subcritical nozzle under different hydrodynamic decay coefficients and stagnation temperature ratios (θ). For the adiabatic case ($\theta = 1.0$), all the responses coincide with those of Marble and Candel [14]. The response amplitude is clearly reduced by increasing either of the cooling rate or hydrodynamic decay in a linear fashion. The slope is almost the same for all cases. In the usual frequency range of the entropy waves (less than few hundred Hz) [35], the entropy wavelength is comparable with the turbulent integral scale of the flow [27]. As a result, in the current study, the decay coefficients (k_n) are assigned small values (less than 10%). Fig. 7a indicates that for $M = 0.025$, by mitigating 10% of the amplitude of the incident entropy wave, P_2^+ reduces by 50 and 45% at $\theta = 0.9$ and $\theta = 1.0$, respectively. It could be, clearly, seen in Fig. 7a and b that the attenuation of the response becomes stronger at higher inlet Mach numbers. This arises from the fact that by increasing the inlet and fixing the outlet Mach number, the velocity (and therefore the pressure) gradient through the nozzle decreases. Hence, conversion of entropy waves to sound declines. It is inferred from Fig. 7a–c that hydrodynamic mechanisms and cooling have comparable effects upon the amplitude of the transmitted acoustic wave, i.e. P_2^+. It is, further, clear from these figures that the absolute value of the P_2^+ is Mach number dependent. However, its reduction due to cooling and hydrodynamics features little sensitivity to the inlet Mach number. In keeping with others [23,59], Figs. 5 and 7 confirm that, in general, the acoustic response of the subsonic nozzle is much stronger than its entropic response.

The amplitude ratio of the outlet to the inlet entropy waves in a subcritical nozzle have been shown in Fig. 8. In Fig. 8, this value has been plotted for different hydrodynamic decay coefficient and a range of stagnation temperature ratios. As expected, for zero hydrodynamic decay and adiabatic nozzle there is no reduction in the amplitude of the entropy wave. It is clear from Fig. 8 that the hydrodynamic decay has a strong influence on the attenuation of the entropy wave, while the cooling effects are less pronounced.

Fig. 9 shows the amplitude of the transmitted wave for different inlet Mach numbers and decay coefficients in the supercritical regime of a nozzle with the incident entropic wave. Once again, the responses under adiabatic condition and for no hydrodynamic decay coincide with those of Marble and Candel [14]. This figure shows that, in general, by decreasing θ the transmitted response is intensified. This means that cooling results in strengthening of the transmitted entropy waves (P_2^+ and P_2^-). This is due to increasing the outlet Mach number and magnifying the pressure gradient through the nozzle, which enhances the conversion of entropy waves into acoustic waves. Figs. 7 and 9 show that in comparison with the subcritical nozzle, the supercritical nozzle is less affected by the hydrodynamic mechanisms. For instance, by diminishing 10% of the entropy wave ($k_n = 0.1$) for $\theta = 0.9$, 14–17 and more than 50% decrements are observed in the amplitude of P_2^+in the supercritical and subcritical nozzles, respectively.

The ratio of the outlet to inlet entropy waves for the supercritical nozzle is depicted in Fig. 10. As expected, the values of the amplitude ratio at the adiabatic case tend to $1 - k_n$. Similar to that discussed for the subcritical nozzle, Fig. 10 shows that under supercritical condition both hydrodynamic decay and cooling have considerable effects on the attenuation of the entropy wave. However, the cooling effects in the supercritical case appear to have stronger effects compared to those in the subcritical nozzle.

6.3. Phase response of the entropy wave in a non-compact nozzle-stretch effects

As stated earlier, due to flow acceleration in the nozzle different parts of the entropy wave may experience different velocities. This stretches the waves and runs a dispersion process. The dependency of the stretch to the governing parameters can be determined through the analysis presented in Section 3. The resultant transfer function under varying inlet Mach numbers in both subcritical and supercritical nozzles are discussed here.

Figs. 11 and 12 show the transfer function of the entropy wave calculate by Eq. (54) for $\Delta\tau/\tau = 0.25$ and 0.5, respectively. The amplitude and phase of the transfer function have been presented for both subcritical and supercritical cases. It is observed, in these figures, that by increasing the wave width, the phase change is intensified in both subcritical and supercritical cases. Figs. 11 and 12 clearly show the strong effect of the wave frequency, and therefore wavelength, upon the amplitude attenuation by the stretch effects. Furthermore, the variation of the inlet Mach number has a strong effect on the entropy transfer function in the subcritical nozzle. For instance, by decreasing Mach number for $\Delta\tau/\tau = 0.25$, the phase increment is 32 and 10% in subcritical and supercritical conditions, respectively. Further, these values for $\Delta\tau/\tau = 0.5$ become 69 and 38%. This raises from the velocity (and then the pressure) gradient throughout the nozzle. When the inlet velocity decreases, the velocity gradient increases and the stretch effect rises. However, the gradient does not increase significantly for the investigated inlet Mach numbers of the supercritical nozzle. As expected, for all cases the phase shows the characteristics of a classical convective lag with lower slopes at higher inlet Mach numbers. It can be simply

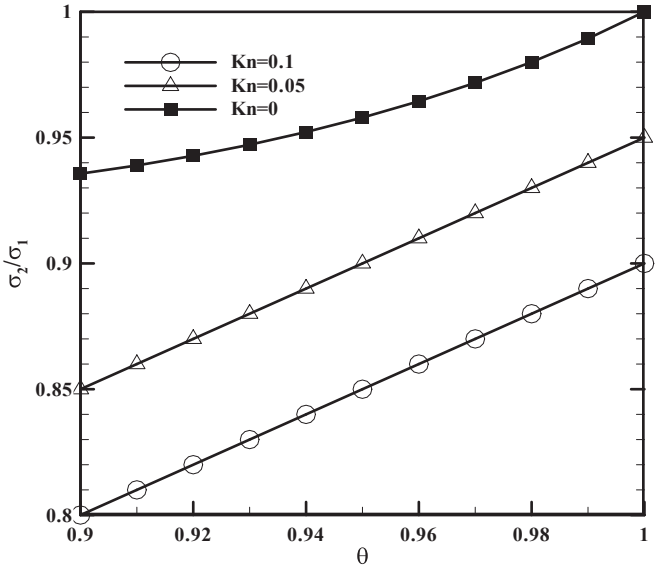

Fig. 10. Ratio of the outlet to inlet entropy waves (σ_2/σ_1) for different hydrodynamic decays and inlet to outlet stagnation temperature ratio.

verified that the convection delay calculated from the slope of the phase graphs corresponds to the average residence time of the entropy wave inside the nozzle.

Figs. 11 and 12 show that the amplitude of the transfer function decays rapidly as the non-dimensional frequency increases. This fall of the amplitude is significant in both cases studied in these figures. Nonetheless, the case with larger temporal width, shown in Fig. 12, appears to feature a quicker decay. In either case the initial decay of the amplitude is followed by a series of peaks and troughs. The change in the Mach number modifies the locations of these peaks and troughs. Although the inlet Mach number can modify the amplitude ratio considerably, the general qualitative behaviour of the transfer function remains independent of the inlet Mach number. The observed behaviour is of practical significance in the analysis of entropy noise. According to these results, high frequency entropy waves are majorly annihilated by stretch effects, while the low frequency wave can mostly survive. As the frequency approaches zero, the effect of stretch on the entropy wave becomes negligible. This means that in a compact nozzle, the stretch is insignificant due to coinciding the throat and boundaries. By increasing the frequency, the nozzle length becomes comparable to the wavelength and the effect of stretch becomes more pronounced. This behaviour is consistent with the experimental [35], numerical [41] and analytical [26] evidence indicating that only low frequency entropy waves are of practical significance.

6.4. Phase response of non-compact nozzles-heat transfer effects

In this section, the phase response of the acoustic waves in the divergent section of the nozzle is calculated by using the results of the effective length analysis presented in section 3. Similar to the previous investigations [18], the nozzle under supercritical

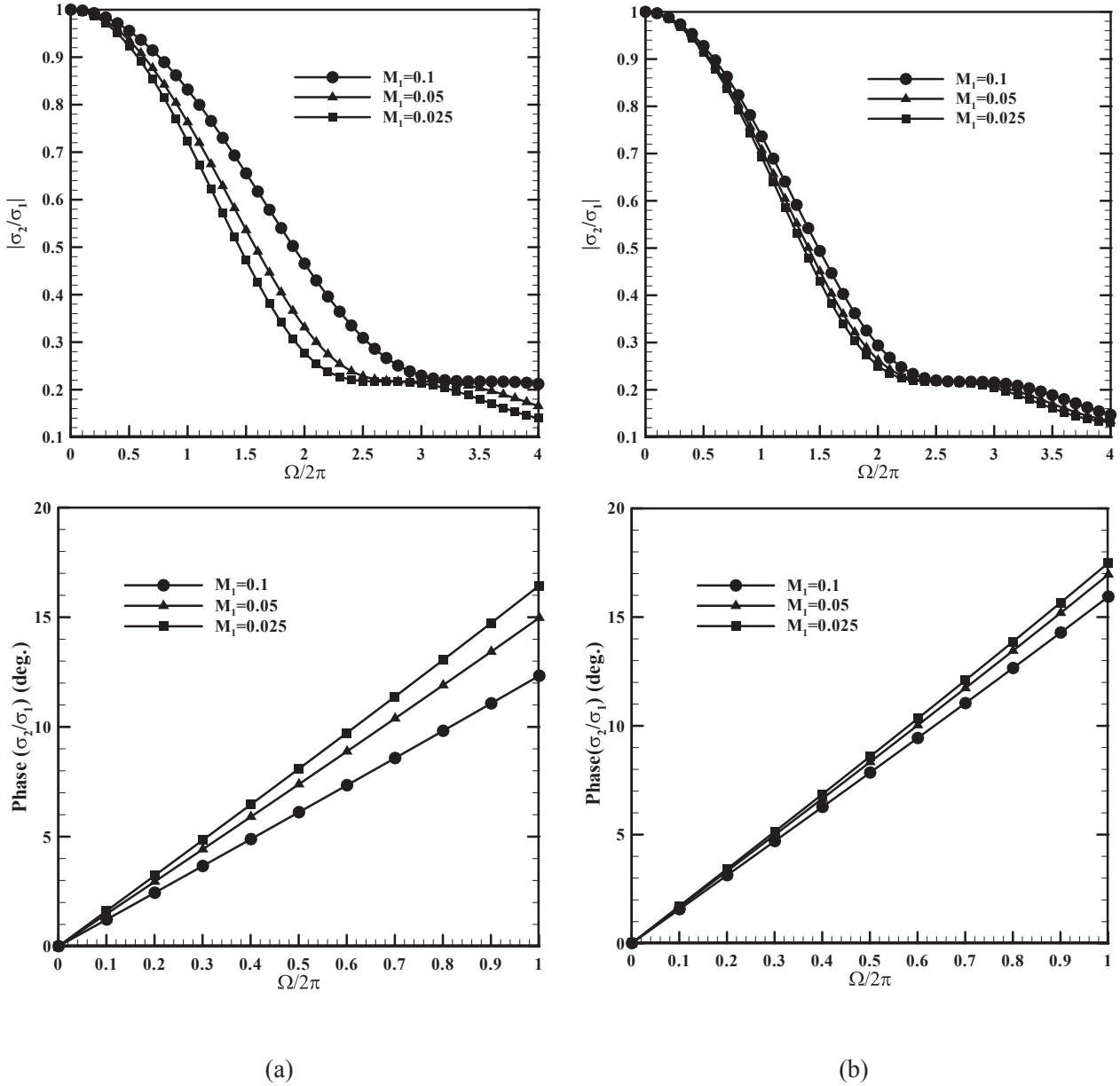

Fig. 11. Transfer function of the of the entropy waves $\left(\frac{\sigma_2}{\sigma_1}\right)$ between the inlet and the throat under varying inlet Mach numbers for $\Delta\tau/\tau = 0.25$ at (a) subcritical and (b) supercritical condition.

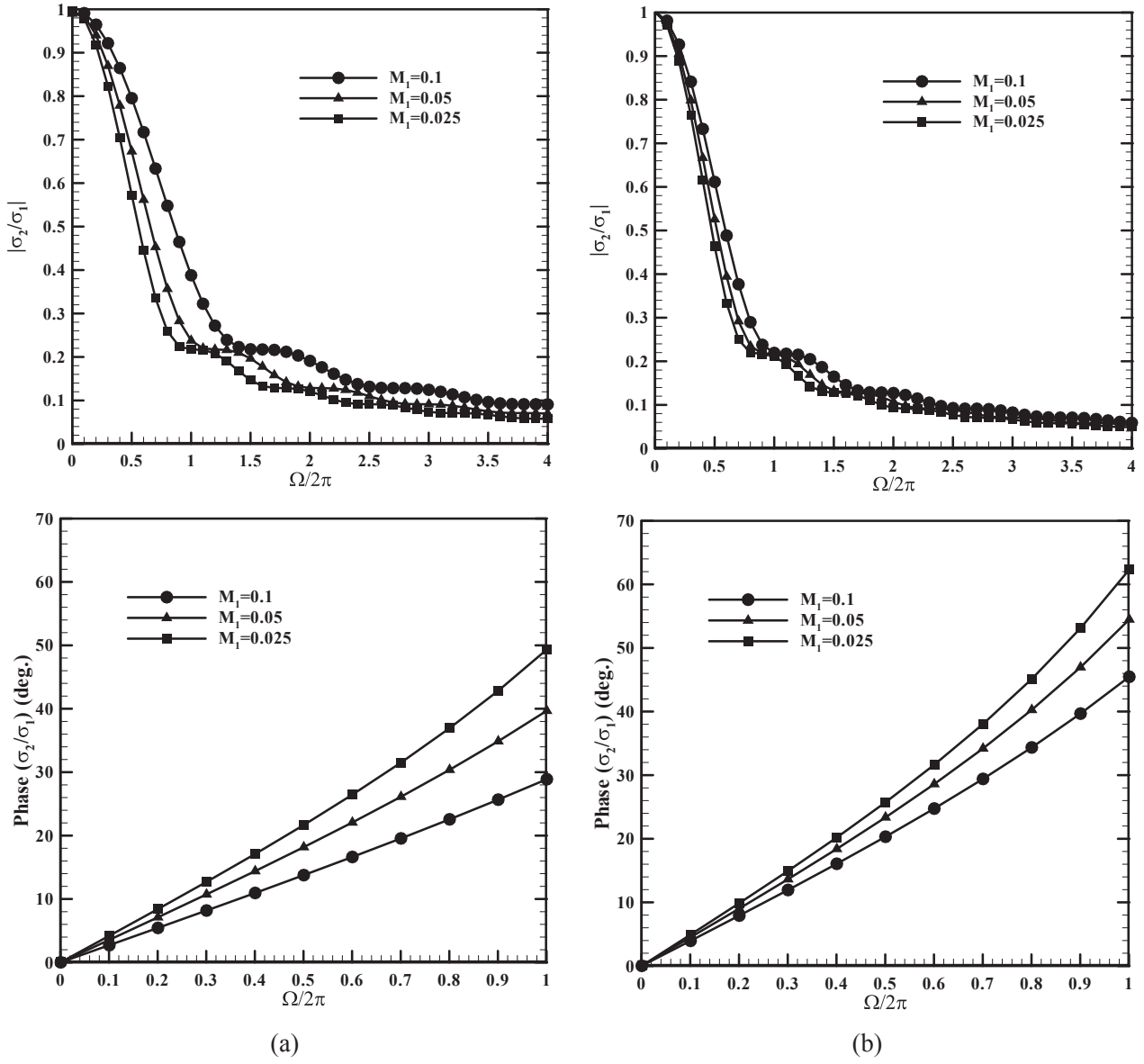

Fig. 12. Transfer function of the entropy waves $\left(\frac{\sigma_2}{\sigma_1}\right)$ between the inlet and the throat under varying inlet Mach numbers for $\Delta\tau/\tau = 0.5$ at (a) subcritical and (b) supercritical condition.

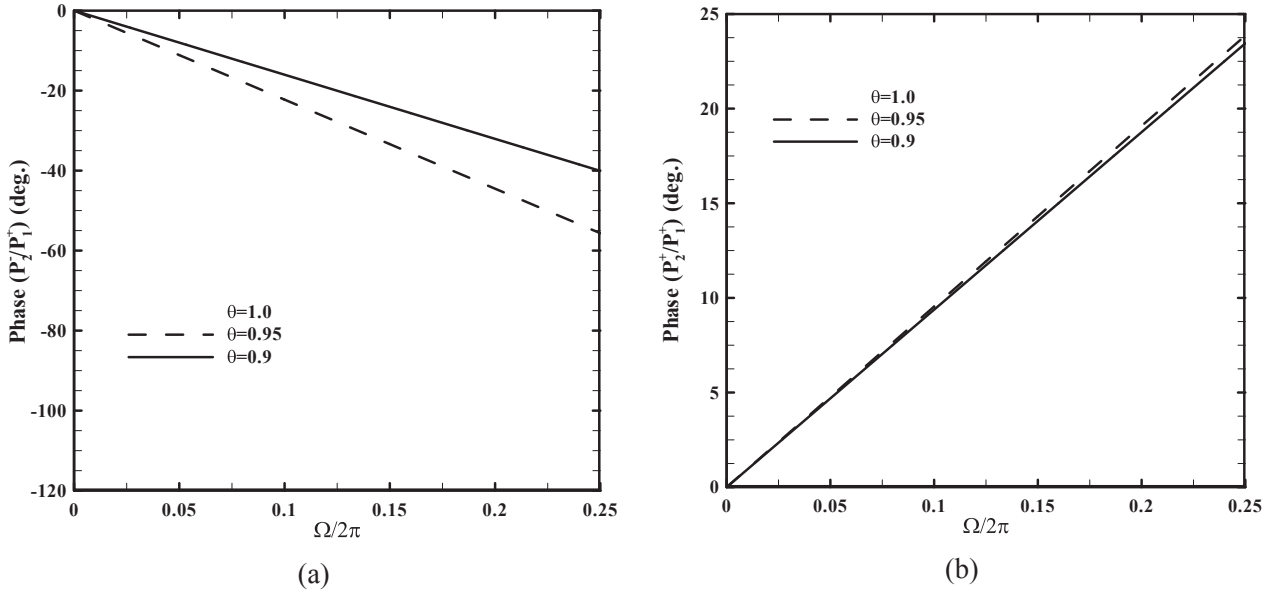

Fig. 13. Phase of the acoustic wave in a supercritical nozzle by an incident acoustic wave: (a) P_2^+/P_1^+, (b) $\frac{P_2^-}{P_1^+}$.

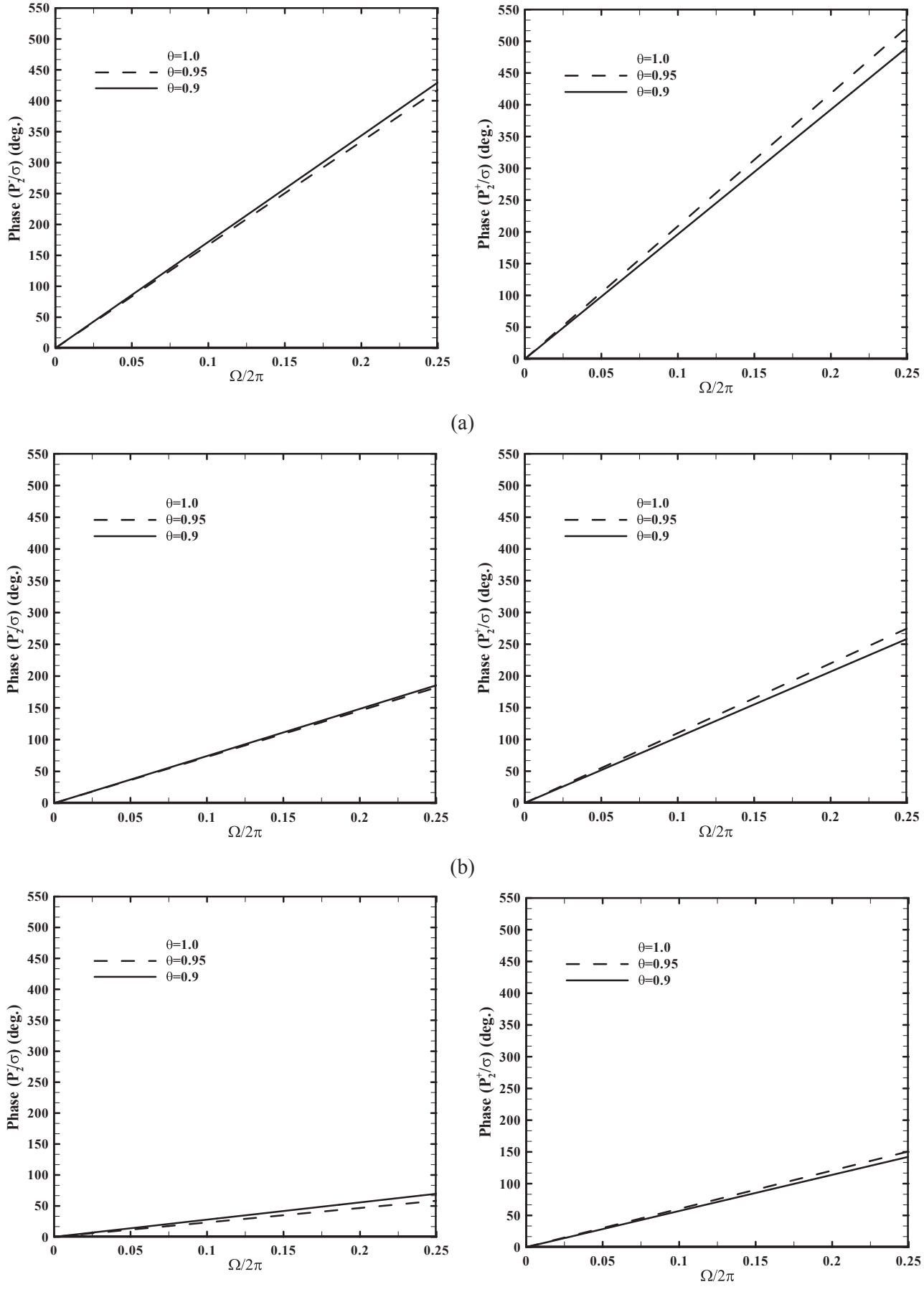

Fig. 14. Transmission and reflection entropy wave (P_2^+/σ and P_2^-/σ) phases in a supercritical nozzle by an incident entropy wave at inlet Mach number of (a) 0.025, (b) 0.05, (c) 0.1.

condition is excited acoustically and entropically.

Fig. 13 shows the phase response of the transmission wave in a nozzle subject to an incident acoustic wave. Fig. 13a shows that by increasing the heat transfer rate (i.e. decreasing θ) there is a significant change in the phase of P_2^-/P_1^+. Nevertheless, within the considered frequency range, the phase change of P_2^+/P_1^+ remains quite small. Thus, it may be concluded that for this acoustically excited nozzle, the phase of P_2^+ is almost insensitive to heat transfer. However, this is not the case for the P_2^-. It could be, readily, verified that increasing the inlet Mach number has negligible effect upon the phase change in Fig. 13 and therefore is not further elaborated here.

Fig. 14 shows the transmission phase in a nozzle with an entropic incident wave and under varying inlet Mach numbers. Although not shown here, it is found that increasing the decay coefficient leaves a negligibly small effect on the phase change. In keeping with the earlier works [18], Fig. 14 shows that the phase of P_2^+/σ and P_2^-/σ feature a linear behaviour as the dimensionless frequency varies.

In general, variation of the phases of P_2^+/σ and P_2^-/σ with respect to frequency is strongly dependent upon the inlet Mach number. For higher inlet Mach numbers (Fig. 14c) the phase variation with frequency is much smaller than that at low inlet Mach number (Fig. 14a). It is also noted that increasing the cooling rate results in the phase decline of P_2^+/σ for all inlet Mach numbers. However, a reverse trend is observed for the phase of P_2^-/σ. The results shown in Figs. 13 and 14 clearly demonstrate the influences of heat transfer on the phase response of pressure waves in the divergent section of the nozzle. As expected, this influence is negligible at frequencies approaching zero. However, it quickly grows with increasing the frequency and becomes appreciable even at relatively low values of the dimensionless frequency.

7. Conclusions

The contribution of entropy noise with combustion instability continues to be a matter of contention. The disagreement has been chiefly caused by neglecting the influences of flow and heat transfer on the entropy wave convecting through the combustor. This paper, therefore, presented a series of analytical studies on the effects of dissipation and dispersion mechanisms upon the transmission and reflection of entropy waves in subcritical and supercritical exit nozzles of hydrogen combustors. These mechanisms are due to the hydrodynamic, heat transfer and flow stretch effects. The compact analysis of Marble and Candel [14] was, first, extended to include heat transfer and hydrodynamic decay of entropy waves. Amplitudes of the reflected and transmitted components were calculated for the acoustically and entropically excited nozzles under varying inlet Mach number, heat transfer rate and hydrodynamic decay. Analytical expressions were, further, derived to find the stretch of convective waves in a nozzle. The concept of effective length was, subsequently, employed to calculate the effects of heat transfer and hydrodynamic decay upon the phase response of the nozzle acoustics.

The main findings of this work can be summarised as follows.

- In keeping with that reported in the recent literature, it was shown that the acoustic responses of the nozzles are stronger than their entropic responses.
- Heat transfer from the nozzle was shown to be able to significantly modify the low frequency response of the subcritical nozzles to acoustic waves. This effect appeared to be weaker in supercritical nozzles.
- The effects of heat transfer and hydrodynamic decay on the reflected and transmitted waves in an entropically excited nozzle could be appreciable.
- The extent of the influences of heat transfer and hydrodynamic effects upon the entropy response were found to be, generally, dependent on the inlet Mach number. This implies that the temperature of combustion products and thus the equivalence ratio of hydrogen and oxidiser mixture can affect the decay of entropy wave. In the investigated supercritical case, the phase of the response was found weakly related to hydrodynamic decay. However, even at relatively low dimensionless frequencies, the influence of heat transfer was considerable.
- It was shown that the dispersion of entropy waves in nozzles is highly frequency dependent. This is such that only low frequency entropy waves can survive the stretch effects of the flow inside the nozzle.
- It is evident from this study that the decay mechanisms of entropy waves can significantly affect their conversion to sound. Thus, inclusion of these mechanisms in the theoretical models of entropy waves appears to be a necessity.

Acknowledgement

Nader Karimi acknowledges the partial support of EPSRC through grant number EP/N020472/1.

References

[1] Morgans AS, Duran I. Entropy noise: a review of theory, progress and challenges. Int J Spray Combust Dyn 2016;8(4):285–98.
[2] Candel S, Durox D, Ducriux S, Birbaud A, Noiray N, Schuller D. Flame dynamics and combustion noise: progress and challenges. Aeroacoustics 2009;8(1&2):1–56.
[3] Candel S, Durox D, Schuller T, Darabiha N, Hakim L, Schmitt T. Advances in combustion and propulsion applications. Eur J Mech B Fluid 2013;40:87–106.
[4] Lieuwen Tim C. Unsteady combustor physics. Cambridge University Press; 2012.
[5] Singh AV, Yu M, Gupta AK, Bryden KM. Thermo-acoustic behavior of a swirl stabilized diffusion flame with heterogeneous sensors. Appl Energy 2013;106:1–16.
[6] Singh AV, Yu M, Gupta AK, Bryden KM. Investigation of noise radiation from a swirl stabilized diffusion flame with an array of microphones. Appl Energy 2013;112:313–24.
[7] Talei M, Hawkes ER, Brear M. A direct numerical simulation study of frequency and Lewis number effects on sound generation by two-dimensional forced laminar premixed flames. Proceedings of the Combustion Institute Proceedings of the Combustion Institute 2013;34(1):1093–100.
[8] Talei M, Brear MJ, Hawkes ER. A comparative study of sound generation by laminar, combusting and non-combusting jet flows. Theor Comput Fluid Dynam 2014;28:385–408.
[9] Karimi N. Response of a conical, laminar premixed flame to low amplitude acoustic forcing- A comparison between experiment and kinematic theories. Energy 2014;78:490–500.
[10] Emadi M, Kaufman K, Burkhalter MW, Salameh T, Gentry T, Ratner A. Examination of thermo-acoustic instability in a low swirl burner. Int J Hydrogen Energy 2015;40(39):13594–603.
[11] Park J, Lee MC. Combustion instability characteristics of H2/CO/CH4 syngases and synthetic natural gases in a partially-premixed gas turbine combustor: Part I—frequency and mode analysis. Int J Hydrogen Energy 2016;41(18):7484–93.
[12] Ffwocs Williams JE, Howe MS. The generation of sound by density inhomogeneities in low Mach number nozzle flows. J Fluid Mech 1975;41:207–32.
[13] Howe M. Contributions to the theory of aerodynamic sound, with application to excess jet noise and the theory of the flute. J Fluid Mech 1975;71:625–73.
[14] Marble FE, Candel SM. Acoustic disturbances from gas non-uniformities convected through a nozzle. J Sound Vib 1977;55(2):225–43.
[15] Cumpsty NA, Marble FE. Core noise from gas turbine exhausts. J Sound Vib 1977;54(2):297–309.
[16] Cumpsty NA. Jet engine combustion noise: pressure, entropy and vorticity perturbations produced by unsteady combustion or heat addition. J Sound Vib 1979;66(4):527–44.
[17] Stow SR, Dowling AP, Hynes TP. Reflection of circumferential modes in a choked nozzle. J Fluid Mech 2002;467:215–39.
[18] Goh CS, Morgans AS. Phase prediction of the response of choked nozzles to entropy and acoustic disturbances. J Sound Vib 2011;330:5184–98.

[19] Moase WH, Brear MJ, Manzie C. The forced response of choked nozzles and supersonic diffusers. J Fluid Mech 2007;585:281–304.
[20] Hosseinalipour SM, Fattahi A, Karimi N. Analytical investigation of non-adiabatic effects on the dynamics of sound reflection and transmission in a combustor. Appl Therm Eng 2016;98:553–67.
[21] Bake F, Kings N, Rohle I. Fundamental mechanism of entropy noise in aero-engines: experimental investigation. J Eng Gas Turbines Power 2008;130(1). 011202-1 - 011202-6.
[22] Bake F, Richter C, Muhlbauer B, Kings N, Rohle I, Thiele F, Noll B. The entropy wave generator (EWG): a reference case on entropy noise. J Sound Vib 2009;326(3–5):574–98.
[23] Leyko M, Moreau S, Nicoud F, Poinsot T. Numerical and analytical modeling of entropy noise in a supersonic nozzle with a shock. J Sound Vib 2011;330:3944–58.
[24] Durán I, Moreau S, Poinsot T. Analytical and numerical study of combustion noise through a subsonic nozzle. AIAA J 2012;51(1):42–52.
[25] Duran I, Leyko M, Moreau S, Nicoud F, Poinsot T. Computing combustion noise by combining large eddy simulations with analytical models for the propagation of waves through turbine blades. Compt Rendus Mec 2013;341:131–40.
[26] Duran I, Moreau S. Solution of the quasi-one-dimensional linearized Euler equations using flow invariants and the Magnus expansion. J Fluid Mech 2013;723:190–231.
[27] Huet M, Giauque A. Nonlinear model for indirect combustion noise through a compact nozzle. J Fluid Mech 2013;733:268–301.
[28] Leyko M, Nicoud F, Poinsot T. Comparison of direct and indirect combustion noise mechanisms in a model combustor. AIAA J 2009;47(11):2709–16.
[29] Fattahi A, Hosseinalipour SM, Karimi N. On the dissipation and dispersion of entropy waves in heat transferring channel flows. Phys Fluids 2017;29(8). 087104.
[30] Mac Quisten MA, Dowling AP. Low-frequency combustion oscillations in a model afterburner. Combust Flame 1993;94:253–64.
[31] Dowling A P. Acoustics of unstable flows. Theoretical and applied mechanics. T. Tatsumi, E. Watanabe, and T. Kambe, eds. Amsterdam: Elsevier; 171-186.
[32] Keller JJ. Thermoacoustic oscillations in combustion chambers of gas turbines. AIAA J 1995;33(12):2280–7.
[33] Zhu M, Dowling AP, Bray KNC. Self excited oscillations in combustors with spray atomizers. Munich: Germany: ASME Turbo Expo; 2000.
[34] Polifke W, Paschereit CO, Dobbeling K. Constructive and destructive interference of acoustic and entropy waves in a premixed combustor with a choked exit. Int J Acoust Vib 2001;6(3):135–46.
[35] Hield PA, Brear MJ, Ho Jin S. Thermoacoustic limit cycles in a premixed laboratory combustor with open and choked exits. Combust Flame 2009;156:1683–97.
[36] Eckstein J, Freitag E, Hirsch C, Sattelmayer T. Experimental study on the role of entropy waves in low-frequency oscillations in a RQL combustor. J Eng Gas Turbines Power 2006;128(2):264–70.
[37] Eckstein J, Sattelmayer T. Low-order modeling of low-frequency combustion instabilities in Aeroengines. J Propuls Power 2006;22(2):425–32.
[38] Sattelmayer T. Influence of the combustor aerodynamics on combustion instabilities from equivalence ratio fluctuations. J Eng Gas Turbines Power 2003;125:11–20.
[39] Hield PA, Brear MJ. Comparison of open and choked premixed combustor exit during thermoacoustic limit cycles. AIAA J 2008;46:517–27.
[40] Brear MJ, Carolan DC, Karimi N. Dynamic response of the exit nozzle of a premixed combustor to acoustic and entropic disturbances. In: The 8th European fluid mechanics Conference. Germany: Bad Reichenhall; 2010.
[41] Morgans AS, Goh CS, Dahan JA. The dissipation and shear dispersion of entropy waves in combustor thermoacoustics. J Fluid Mech 2013:733. R2-1-R2-11.
[42] Rolland EO, De Domenico F, Hochgreb S. Theory and application of reverberated direct and indirect noise. J Fluid Mech 2017 May;819:435–64.
[43] De Domenico F, Rolland EO, Hochgreb S. Detection of direct and indirect noise generated by synthetic hot spots in a duct. J Sound Vib 2017 Apr 28;394:220–36.
[44] Rolland EO, De Domenico F, Hochgreb S. Direct and indirect noise generated by entropic and compositional inhomogeneities. J Eng Gas Turbines Power 2018 Aug 1;140(8). 082604.
[45] De Domenico F, Rolland EO, Hochgreb S. A generalised model for acoustic and entropic transfer function of nozzles with losses. J Sound Vib 2019 Feb 3;440:212–30.
[46] Wassmer D, Schuermans B, Paschereit CO, Moeck JP. Measurement and modeling of the generation and the transport of entropy waves in a model gas turbine combustor. Int J Spray Combust Dyn 2017 Dec;9(4):299–309.
[47] Goh CS, Morgans AS. The influence of entropy waves on the thermoacoustic stability of a model combustor. Combust Sci Technol 2013;185:249–68.
[48] Motheau E, Nicoud F, Poinsot T. Mixed acoustic-entropy combustion instabilities in gas turbines. J Fluid Mech 2014;749:542–76.
[49] Lourier JM, Huber A, Noll B, Aigner M. Numerical analysis of indirect combustion noise generation within a subsonic nozzle. AIAA J 2014;52(10):2114–25.
[50] Magri L, O'Brien J, Ihme M. Compositional inhomogeneities as a source of indirect combustion noise. J Fluid Mech 2016 Jul:799.
[51] Karimi N, Brear M, Moase W. Acoustic and disturbance energy analysis of a flow with heat communication. J Fluid Mech 2008;597:67–89.
[52] Karimi N, Brear M, Moase W. On the interaction of sound with steady heat communicating flows. J Sound Vib 2010;329(22):4705–18.
[53] Howe MS. Indirect combustion noise. J Fluid Mech 2010;659:267–88.
[54] Motheau E, Selle L, Nicoud F. Accounting for convective effects in zero-Mach-number thermoacoustic models. J Sound Vib 2014;333:246–62.
[55] John JE, Theo GK. Gas dynamics. Pearson Prentice Hall; 2006.
[56] Shapiro AH. The dynamics and thermodynamics of compressible fluid flow, vol. 1. New York: The Ronald Press Company; 1953.
[57] Turns SR. An introduction to combustion. New York: McGraw-hill; 1996.
[58] Van Wylen GJ, Sonntag RE, Borgnakke C. Fundamentals of thermodynamics. sixth ed. Wiley; 1986.
[59] Giauque A, Huet M, Clero F. Analytical analysis of indirect combustion noise in subcritical nozzles. J Eng Gas Turbines Power 2012;134. 11202-1-8.